Cell Reports

Article

m6A modification inhibits miRNAs' intracellular function, favoring their extracellular export for intercellular communication

Graphical abstract

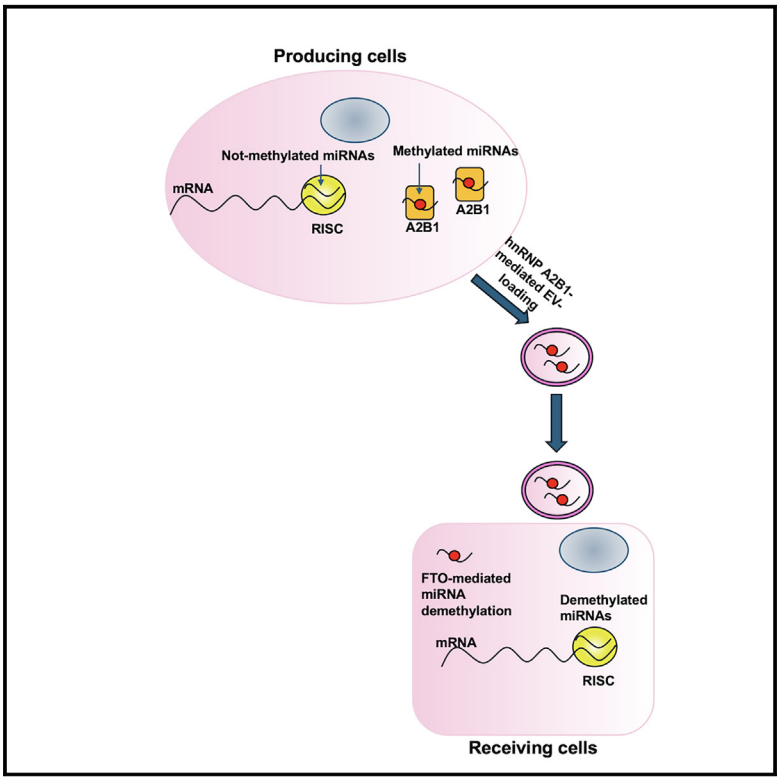

Highlights

- Mature miRNAs are m6A modified in a cell-specific manner
- m6A modification impairs methylated miRNAs/AGO2 interaction and, in turn, miRNA function
- miRNA m6A modification enhances their EV compartmentalization through the EV-loader A2B1
- Recipient cells utilize EV-miRNA informational content in dependence on FTO demethylation

Authors

Sabrina Garbo, Daniel D'Andrea, Alessio Colantoni, ..., Andrea Tancredi, Marco Tripodi, Cecilia Battistelli

Correspondence

marco.tripodi@uniroma1.it (M.T.), cecilia.battistelli@uniroma1.it (C.B.)

In brief

Garbo et al. report that mature miRNAs are methylated (m6A) in a cell-specific manner and that highly methylated miRNAs are impaired in AGO2 association and in their intracellular function. m6A modification enhances extracellular vesicle (EV) A2B1-mediated compartmentalization. Notably, receiving cells demethylate EV-delivered miRNAs and restore their function.

Garbo et al., 2024, Cell Reports *43*, 114369
June 25, 2024
https://doi.org/10.1016/j.celrep.2024.114369

CellPress

Cell Reports

CellPress
OPEN ACCESS

Article

m6A modification inhibits miRNAs' intracellular function, favoring their extracellular export for intercellular communication

Sabrina Garbo,[1] Daniel D'Andrea,[2] Alessio Colantoni,[3] Francesco Fiorentino,[4] Antonello Mai,[5] Andres Ramos,[6] Gian Gaetano Tartaglia,[7] Andrea Tancredi,[8] Marco Tripodi,[1,9,*] and Cecilia Battistelli[1,9,10,*]

[1]Istituto Pasteur Italia-Fondazione Cenci Bolognetti, Department of Molecular Medicine, Sapienza University of Rome, Viale Regina Elena 324, 00161 Rome, Italy
[2]School of Science and Technology, Nottingham Trent University, Clifton Campus, Nottingham NG11 8NS, UK
[3]Department of Biology and Biotechnologies "Charles Darwin", Sapienza University of Rome, 00185 Rome, Italy
[4]Center for Life Nano- and Neuro-Science, RNA Systems Biology Lab, Fondazione Istituto Italiano di Tecnologia (IIT), 00161 Rome, Italy
[5]Department of Drug Chemistry and Technologies Sapienza University of Rome, Ple. Aldo Moro 5, 00185 Rome, Italy
[6]Research Department of Structural and Molecular Biology, University College London, Darwin Building, Gower Street, London WC1E 6XA, UK
[7]Center for Human Technologies, Istituto Italiano di Tecnologia, Via Enrico Melen, 83, 16152 Genova, Italy
[8]Dipartimento Metodi e Modelli per l'Economia, il Territorio e la Finanza MEMOTEF, Sapienza University of Rome, 00185 Rome, Italy
[9]These authors contributed equally
[10]Lead contact
*Correspondence: marco.tripodi@uniroma1.it (M.T.), cecilia.battistelli@uniroma1.it (C.B.)
https://doi.org/10.1016/j.celrep.2024.114369

SUMMARY

Epitranscriptomics represents a further layer of gene expression regulation. Specifically, N6-methyladenosine (m6A) regulates RNA maturation, stability, degradation, and translation. Regarding microRNAs (miRNAs), while it has been reported that m6A impacts their biogenesis, the functional effects on mature miRNAs remain unclear. Here, we show that m6A modification on specific miRNAs weakens their coupling to AGO2, impairs their function on target mRNAs, determines their delivery into extracellular vesicles (EVs), and provides functional information to receiving cells. Mechanistically, the intracellular functional impairment is caused by m6A-mediated inhibition of AGO2/miRNA interaction, the EV loading is favored by m6A-mediated recognition by the RNA-binding protein (RBP) hnRNPA2B1, and the EV-miRNA function in the receiving cell requires their FTO-mediated demethylation. Consequently, cells express specific miRNAs that do not impact endogenous transcripts but provide regulatory information for cell-to-cell communication. This highlights that a further level of complexity should be considered when relating cellular dynamics to specific miRNAs.

INTRODUCTION

RNA modification, also known as epitranscriptomics, is an important layer of gene expression regulation that impacts multiple important events in RNA metabolism and function, and it has been prevalently observed on the most abundant RNAs (small nuclear RNAs, tRNAs, and rRNAs). More recently, thanks to the advancements in detection techniques, several modifications have also been characterized on less abundant non-coding RNAs (ncRNAs), including microRNAs, Piwi-interacting RNAs, and long intergenic non-coding RNAs.[1–3] In mRNAs, RNA modifications have been demonstrated to affect stability, splicing, export, decay, and translation, while, with respect to ncRNAs, they have been mainly associated with microRNA (miRNA) biogenesis[4–6] and ncRNA interaction with RNA-binding proteins (RBPs), impacting their function in the chromatin context.[7–9] The methylation status of mature miRNAs has been explored only partially, and its functional significance remains speculative.[2] Here, we address these last issues. Specifically, the dynamic and reversible N6-methyladenosine (m6A), the addition of a methyl group to carbon 6 of adenosine, is the most abundant internal modification in mRNAs and the best characterized[10–12]; it is catalyzed by the methyltransferase-like 3 (METTL3) subunit of the METTL3/METTL14 complex,[13] whose enrichment and sequence specificity on RNA targets has been characterized in detail,[11,13–17] and decoded by reader proteins (e.g., YT homology family members[18] and heterogeneous nuclear ribonucleoprotein [hnRNP] A2B1[4]) and removed by the erasers (e.g., ALKBH5[19] and fat mass and obesity-related [FTO][20]). Notably, while m6A methylation of mRNAs is well dissected, the impact of this methylation on the function of other RNA classes needs to be explored in depth. Here, we combine transcriptome-wide analyses, miRNA-specific biochemical assays, and functional

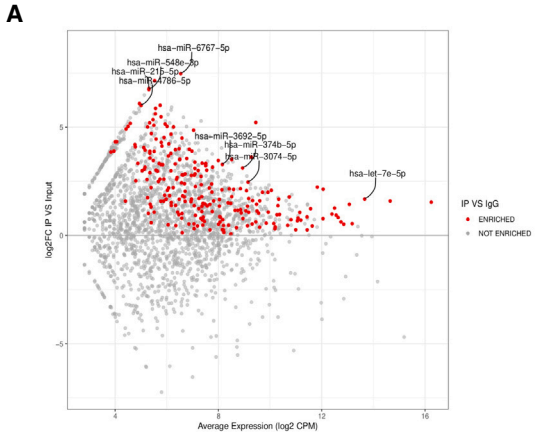

miRNA	sequence	miRNA database
hsa-miR-6767-5p	UCGCAGACAGGGACACAUGGAGA	miRBase
hsa-miR-548e-3p	AAAAACUGAGACUACUUUUGCA	miRBase HC
hsa-miR-215-5p	AUGACCUAUGAAUUGACAGAC	miRBase HC
hsa-miR-4786-5p	UGAGACCAGGACUGGAUGCACC	miRBase HC
hsa-miR-3619-3p	GGGACCAUCCUGCCUGCUGUGG	miRBase HC, MirGeneDB
hsa-miR-3074-5p	GUUCCUGCUGAACUGAGCCAG	miRBase
hsa-miR-374b-5p	AUAUAAUACAACCUGCUAAGUG	miRBase HC, MirGeneDB
hsa-miR-let-7e-5p	UGAGGUAGGAGGUUGUAUAGUU	miRBase HC, MirGeneDB
hsa-miR-3692-5p	CCUGCUGGUCAGGAGUGGAUACUG	miRBase
hsa-miR-28-5p	AAGGAGCUCACAGUCUAUUGAG	miRBase HC, MirGeneDB
hsa-miR-122-5p	UGGAGUGUGACAAUGGUGUUUG	miRBase, MirGeneDB
hsa-miR-301b-5p	GCUCUGACGAGGUUGCACUACU	miRBase
hsa-miR-199a-5p	CCCAGUGUUCAGACUACCUGUUC	miRBase, MirGeneDB
hsa-miR-1180-3p	UUUCCGGCUCGCGUGGGUGUGU	miRBase, MirGeneDB

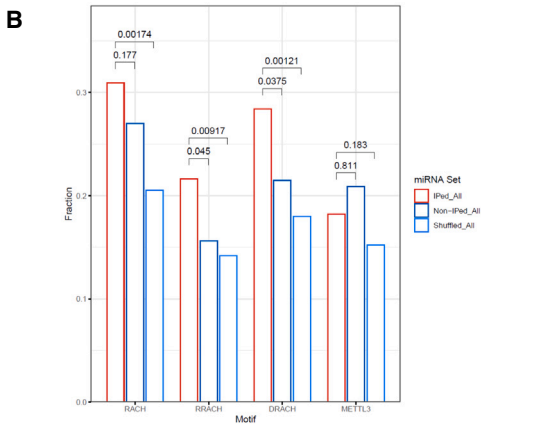

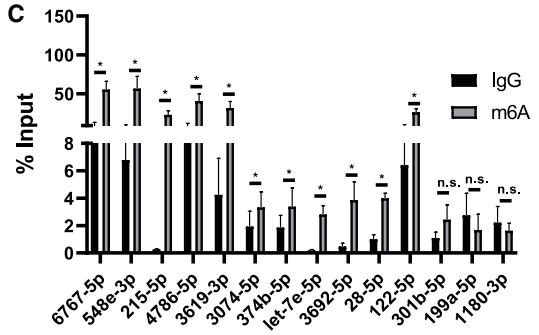

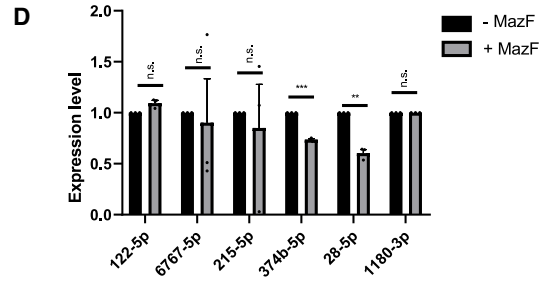

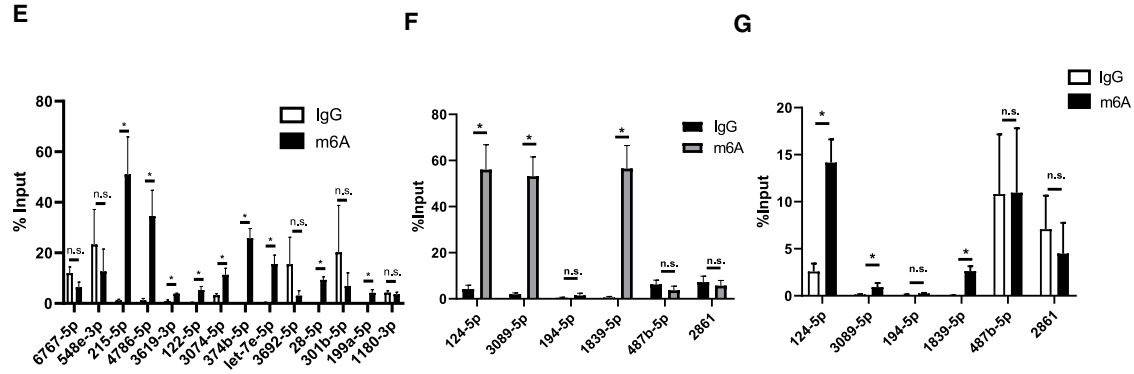

(legend on next page)

experiments to show that these writers, readers, and erasers influence intracellular miRNA function and extracellular miRNA destiny, favoring their loading in extracellular vesicles (EVs) and mediating miRNA function in recipient cells.

RESULTS

Mature miRNAs are m6A modified in a tissue-specific manner

As a first step to gather insights into m6A methylation on mature miRNAs, m6A-methylated RNA was immunoprecipitated from human METTL3-expressing[21] hepatoma HepG2 cells and sequenced in methylated RNA immunoprecipitation sequencing (MeRIP-seq) assays. To increase the robustness of the analysis, these data were compared with those obtained from HepG2 METTL3-silenced cells (shMETTL3; Figures S1A and S1B; Table S1). As further evidence of METTL3 silencing, the expression of Cyclin G1 (Figure S1C) and cellular proliferation (Figure S1D) were found to be attenuated, in accordance with Barbieri et al.[22]; moreover, specific methylated mRNAs[23] provided a further control of immunoprecipitation (IP) (Figure S1E).

Notably, among the sequenced miRNAs, several (i.e., 236 annotated in miRbase 22.1,[24] 119 of which are classified as high confidence in miRbase and/or are also present in the miRGeneDB 2.1 database[25]) display significant levels of m6A modification (log2 fold change [FC] and adjusted p-value for the IP/immunoglobulin G [IgG] comparison $p > 0$ and $p < 0.05$, respectively; log2 FC for the IP/input comparison $p > 0$) and are not enriched in the IP fraction when METTL3 is silenced (shMETTL3_IP vs. shMETTL3 IgG adjusted $p \geq 0.05$ and/or log2 FC < 0) (Figure 1A, left; Table S1).

The occurrence in the immunoprecipitated (IPed) miRNA sets of previously characterized motifs associated with m6A sites (i.e., RACH, RRACH, DRACH, and METTL3;[9,11,14–17] Table S1) was evaluated as compared to two controls sets, one composed of non-IPed miRNAs with expression levels within the range of the IPed ones and the other obtained by randomly shuffling the sequences of the IPed miRNAs. As shown in Figure 1B, RACH, RRACH, and DRACH motifs (but not the METTL3 one) are significantly enriched in the IPed miRNA set, with the RACH motif being found in ~31% of the IPed miRNAs and in ~33% of the IPed miRNA subset composed of 119 high-confidence (HC) miRNAs.

Moreover, the percentage of methylation of specific miRNAs (Figure 1A, right) was evaluated by means of qPCR (Figure 1C); here, estimation of the methylated miRNA fraction was performed by the ratio of IP/input (% input), allowing us to quantify the fraction of each miRNA species that is methylated with respect to the amount of miRNA expressed in the cell. These analyses allowed us to distinguish among high (miRs 6767-5p, 548e-3p, 215-5p, 4786-5p, 3619-3p, and the liver specific 122-5p), low (miRs 3074-5p, 374b-5p, let7e-5p 3692-5p, and 28-5p) and non-methylated miRNAs (miRs 301b-3p, 199a-5p, and 1180-3p, with the last not containing As). As a further proof of concept of methylation, we made use of the MazF assay, consisting of m6A-sensitive RNA endonuclease digestion (where the ACA sequences are cut if not methylated).

Overall, this analysis confirms MeRIP qPCR data in an antibody-independent assay. The three miRNAs 122-5p, 6767-5p, and 215-5p bear an ACA sequence and, being highly methylated, are not cleaved; the miRNAs 374b-5p and 28-5p bear an ACA sequence and, being lowly methylated, are partially cleaved; and 1180-3p (no A bases, negative control) is not cut by MazF (Figure 1D).

The MeRIP qPCR analysis for the same miRNAs was also performed on the human hepatoma cell line Hep3B, thus highlighting different levels of methylation (Figure 1E). Finally, MeRIP qPCR analysis of miRNAs selected for the presence of the methylation motifs (Table S2) was performed on murine livers and murine BW1J cells (Figures 1F and 1G, respectively). As for the two human cell lines, murine cells highlighted different levels of methylation for specific miRNAs, allowing us to conclude that distinct cells show a cell-specific methylation pattern. The miRNA methylation pattern is not simply a reflection of a higher expression, as indicated by these specific miRNAs; the highly expressed miRNAs let-7e-5p, 1180-3p, and 374b-5p are not highly methylated, and, vice versa, the highly methylated miRNAs 6767-5p, 548e-3p, 215-5p, 4786-5p, 3619-3p, and 122-5p are not highly expressed (Figure S2A).

Figure 1. miRNAs are differentially m6A modified

(A) Left: scatterplot showing the average abundance and the log2 FC values for each miRNA, as calculated through limma analysis of the HepG2 MeRIP-seq IP/input comparison. The red dots correspond to miRNAs with IP/input log2 FC > 0 that are enriched (log2 FC > 0 and adjusted $p < 0.05$) in the IP/IgG comparison of shCTR HepG2 cells but not in the IP/IgG comparison of shMETTL3 HepG2 cells. Labeled miRNAs were analyzed in the reported experiments. The x axis shows the average expression values in log2-transformed counts per million reads. For each miRNA, the average expression was calculated across all samples ($n = 4$), with 2 replicates per condition tested. Right: list of miRNAs selected from MeRIP-seq analysis.

(B) Left: barplots showing the fraction of immunoprecipitated (IPed) miRNAs and controls (non-IPed and shuffled miRNAs) that contain at least one m6A motif. The p values reported in the plot were calculated using Fisher's exact test to evaluate the differences in proportions between IPed miRNAs and control sets. Motif enrichment was assessed both for the complete set of IPed miRNAs (left) and for the HC ones (right).

(C) MeRIP-qPCR analysis on 14 miRNAs (301b-5p, 199a-5p, and 1180-3p were negative controls) from HepG2 cells. Data are shown as the mean ± SEM of six independent experiments and are represented as % input.

(D) MazF-qPCR levels on the indicated miRNAs. The unmethylated miR-1180-3p, devoid of As, was used as a negative control. Data are shown as the mean ± SEM of three independent experiments.

(E) MeRIP-qPCR analysis on miRNAs from human Hep3B cells. Data are shown as the mean ± SEM of six independent experiments and are reported as % input.

(F) MeRIP-qPCR analysis on miRNAs from mouse livers. Data are relative to six independent experiments and are shown as in (E).

(G) MeRIP-qPCR analysis on miRNAs from murine BW1J cells. Data are relative to six independent experiments and are shown as in (E).

(F and G) The unmethylated miR-2861, devoid of As, was used as negative control.

(C and E–G) Data are considered statistically significant with $p < 0.05$ (two-tailed Mann-Whitney paired test).

p value: * < 0.05; ** < 0.01; *** < 0.001.

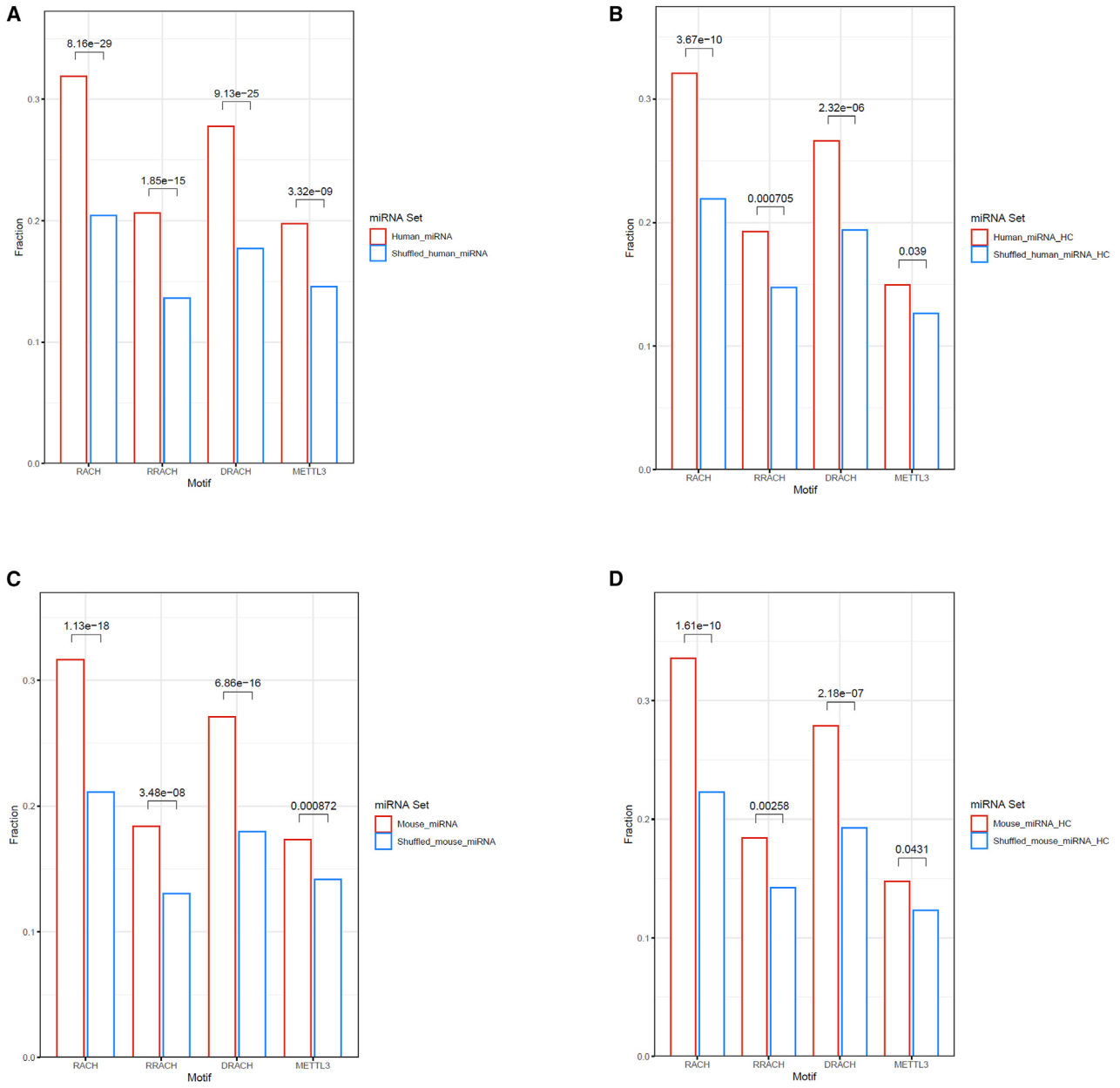

Figure 2. m6A consensus sequences in the human and murine miRNome

(A–D) Barplots showing the fraction of mature miRNAs and shuffled miRNA sequences that contain at least one m6A motif. The *p* values reported in the plot were calculated using Fisher's exact test to evaluate the differences in proportions between miRNAs and controls. Motif enrichment was assessed for the complete (A) and HC (B) sets of human mature miRNAs as well as for the complete (C) and HC (D) sets of murine mature miRNAs.

Notably, we observed a substantial enrichment of m6A consensus motifs within the full human mature miRNA set (Figure 2A; Table S2); e.g., the RACH motif is present in ~32% of human mature miRNAs. This enrichment remains consistent even when restricting the motif enrichment analysis to the human HC miRNAs (Figure 2B). A similar trend was also observed for murine miRNAs (Figures 2C and 2D; Table S2).

These findings suggest that many miRNAs could, in principle, be methylated in a dynamic manner in different cell types.

Mature miRNAs are functionally impaired by m6A modification

These findings prompted us to address the impact of m6A on miRNA function. Since METTL3 silencing impacts gene expression at several levels, specific evidence on miRNA function was gathered by means of a selective approach. Luciferase vectors (Figure 3A, left) containing the 3′ UTR of mRNAs targeted by the miRs 122-5p, 6767-5p, 548e-3p, 301b-5p, and 1180-3p (with the last two as negative controls) were expressed in short

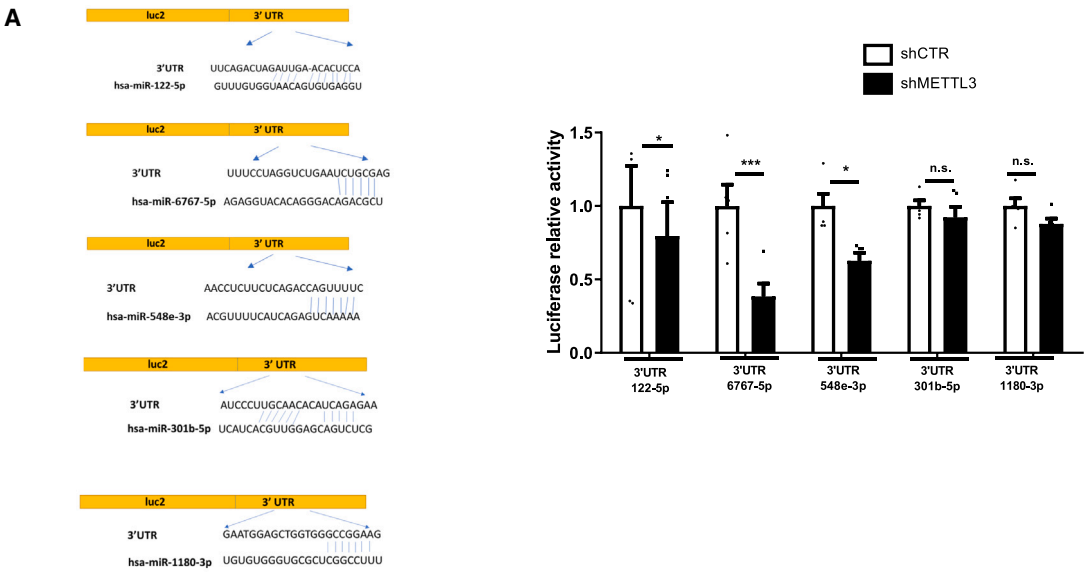

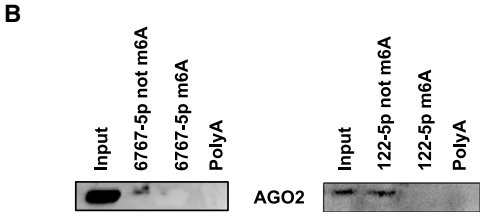

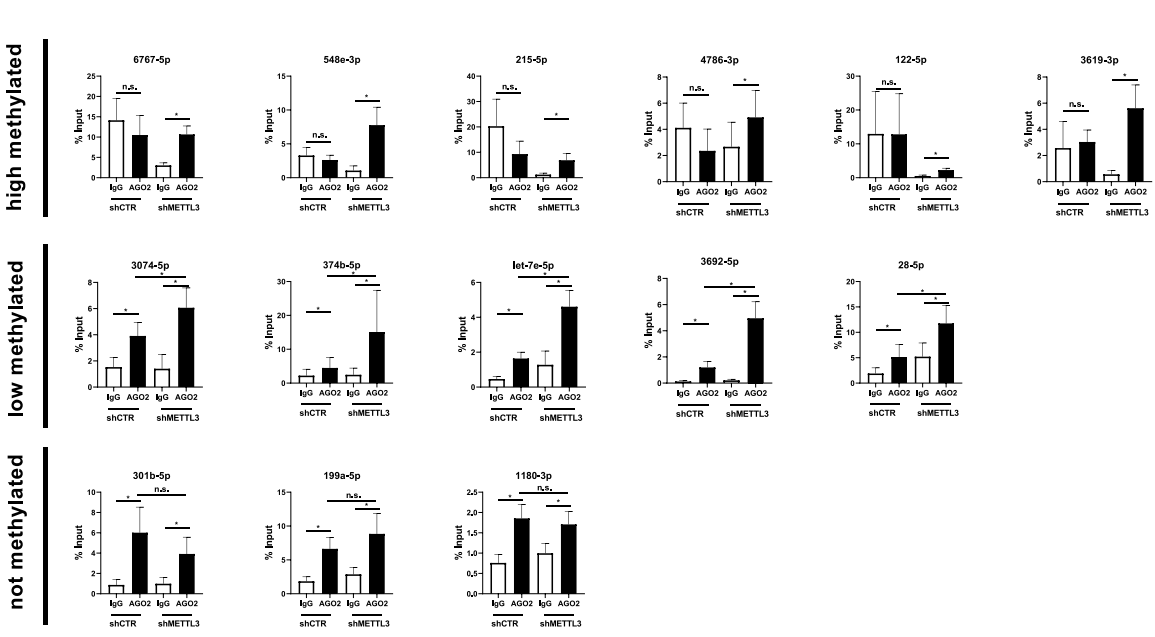

(legend on next page)

hairpin control (shCTR) and shMETTL3 HepG2 cells. Notably, METTL3 silencing lowered the luciferase activity for the highly methylated miR-122-5p, 6767-5p, and 548e-3p, indicating that miRNA function is enhanced upon METTL3 silencing (Figure 3A, right); potential effects of METTL3 depletion directly on the 3′ UTR target were estimated by luciferase assay performed under the same experimental conditions in the presence of the specific antagomiR targeting miR122-5p. As shown in Figure S2B, the result indicates a significant rescue of luciferase activity caused by the miRNA silencing, highlighting that m6A modification impacts miRNA function more than the mRNA target.

Next, we wondered whether the regulatory effect of m6A on miRNA function we observe may derive from m6A affecting the miRNA/AGO2 association; indeed, the impact of methylation on AGO2-miRNA association, while previously proposed by bioinformatic prediction on miR17-5p and let-7a-5p,[2] has not been previously characterized. To test this hypothetic mechanism, an *in vitro* analysis by RNA pull-down was performed on methylated miRs 6767-5p and 122-5p, which showed lower association with AGO2 with respect to the unmethylated form (Figure 3B). RNA IP of AGO2-bound RNA followed by qPCR validation highlighted an inverse correlation between miRNA methylation levels and AGO2 binding, thus indicating that methylation impairs miRNA/RNA-induced silencing complex (RISC) interaction (Figure 3C). Notably, METTL3 silencing (Figures S1A and S1B) significantly restores interaction with AGO2 for all highly methylated miRNAs analyzed (Figure 3C) without impairing AGO2 expression or IP efficiency (Figures S3A and S3B). These data demonstrate that miRNA function is impaired by m6A modification and that METTL3 silencing enhances miRNA activity by restoring miRNA interaction with AGO2.

Overall, these data indicate that several mature miRNAs are targets of methylation and that the highly m6A-modified miRNA fraction is functionally impaired. We next investigated the conceivable hypothesis that methylation influenced miRNA compartmentalization.

m6A modification influences miRNA extracellular compartmentalization

Previous findings have unveiled cellular machineries capable of specifically loading EVs with specific miRNAs by means of specific RBPs (i.e., SYNCRIP,[26] A2B1,[27] FUS, and ALY[28]). Here, we asked whether m6A modification may also have an impact on miRNA extracellular compartmentalization.

Firstly, we verified, by RNA dot blot and native mass spectrometry, whether m6A-modified miRNAs were significantly enriched within purified EVs (Figures S4A–S4D). In order to estimate specific miRNAs' methylation, several were tested by meRIP-qPCR analysis.

As shown in Figure 4A, m6A modification levels of specific miRNAs in EVs are higher than in the intracellular compartment, and METTL3 silencing results in a reduction in their loading in EVs (Figure 4B). Furthermore, miRNAs found to be unmethylated in the cellular compartment (miR 301b-5p and 199a-5p) are found to be methylated in EVs. This depends on METTL3 catalytic activity, as demonstrated by the effect of the METTL3-specific inhibitor STM2457[23] (Figure 4C). Overall, these data indicate that m6A is a functional hallmark of EV export of a subset of miRNAs.

m6A modification influences RNA binding protein-mediated miRNA loading in the EVs

To define a molecular rationale for this observation, we explored whether m6A methylation may regulate one of the known pathways involved in miRNA loading into EVs. We focused on hnRNPA2B1 (A2B1), which has been shown to recognize m6A methylation[4,29] and is involved in miRNA sorting into EVs.[27]

First, we observed that A2B1 knockdown (Figure S5A) impairs miRNA loading into EVs, thus confirming A2B1 as an important player in this process (Figure 5A). RNA pull-down showed that A2B1 preferentially associates with methylated rather than with unmodified miR-122-5p (Figure 5B), and this *in vitro* evidence has been confirmed in HepG2 cells by A2B1 crosslinking RNA IP (CLIP) followed by qPCR analysis of miRNAs selected through the next-generation sequencing approach, which allowed us to conclude that A2B1 direct interaction with specific miRNAs is influenced by METTL3 silencing (Figure 5C). Therefore, A2B1's ability to bind to miRNAs in a sequence-specific manner is here extended to its ability to act as an m6A reader. In addition, the methylation-dependent A2B1 miRNA-binding and loading functions require its SUMOylation (in line with Villarroya-Beltri et al.[27]), as demonstrated by treatment with the SUMOylation inhibitor ML-792 (Figures S5B and S5C).

Taken together, these data indicate that m6A miRNA modification plays a dual role: it impairs intracellular function and influences extracellular compartmentalization in EVs. Molecular players of these two outcomes were identified here in AGO2 and A2B1, respectively. Conceivably, other RBPs may parallel the A2B1 function identified here in dependence on m6A.

The regulatory layer described here implies that, in future observations, together with miRNA expression levels, their effective intracellular functionality and/or extracellular delivery as implemented by m6A editing should be taken into account. This scenario begets a fresh question: do receiving cells modify EV-miRNA methylation and restore their gene regulation potential?

Figure 3. miRNAs are functionally impaired by m6A modification

(A) Left: luciferase vectors used in luciferase assays. Right: luciferase relative activity in shCTR and shMETTL3 HepG2 cells transfected with luciferase vectors containing a 3′ UTR targeted by miR-122-5p, miR-6767-5p, miR-548e-3p, miR-301b-5p, and miR-1180-3p (with the last used as a negative control). Data are shown as the mean ± SEM of five independent experiments.

(B) RNA pull-down with the methylated and unmethylated miR-6767-5p and miR122-5p, followed by western blot for AGO2. Data are representative of three independent experiments.

(C) CLIP of AGO2 protein in shCTR and shMETTL3 HepG2 cells on differentially methylated miRNAs. Data are shown as the mean ± SEM of six independent experiments and are represented as % input. miR301b-5p, 199a-5p, and 1180-3p are negative controls. Data are considered statistically significant with $p < 0.05$ (two-tailed Mann-Whitney paired test). p value: * < 0.05; ** < 0.01; *** < 0.001.

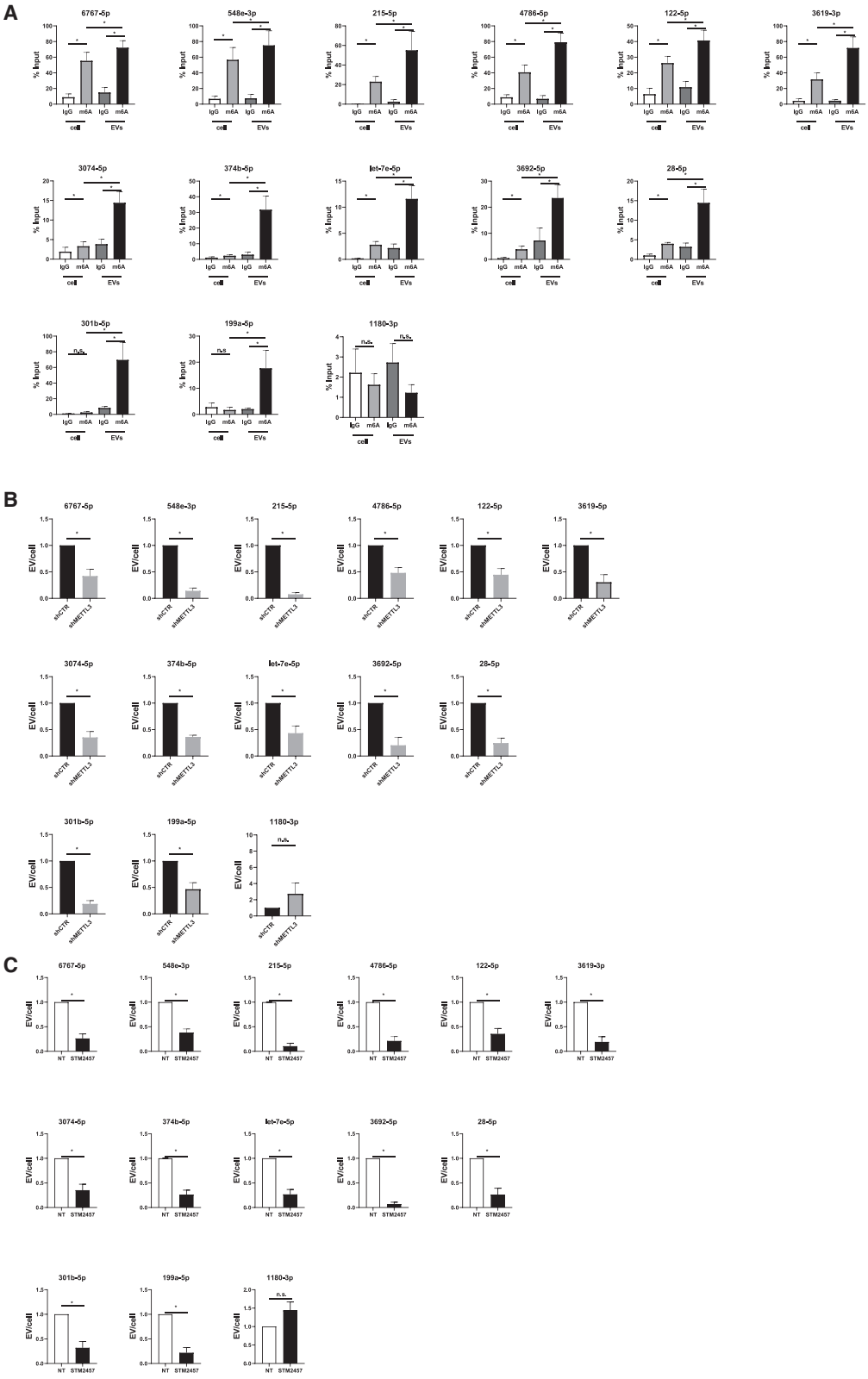

(legend on next page)

EV-miRNA function on recipient cells requires demethylation

To establish whether the m6A-regulated EV-transported miRNAs are functional in the recipient cells, we first compared the functional properties of the EVs derived from producing shCTR and shMETTL3 HepG2 cells on recipient murine hepatocytes.[30] As shown in Table S3, mRNA sequencing of recipient cells provides evidence of a broad EV-mediated mRNA steady-state-level perturbation. Then we focused on specific targets of the high methylated miRNAs and evaluated the level of atp5o and eny2 mRNAs, targeted by miR-215-5p (which has a conserved sequence in human and mouse), using qPCR. The results highlight that the mRNAs are downregulated in response to a treatment with shCTR-derived EVs, while treatment with shMETTL3-derived EVs has a lower effect (Figure 6A). Further proof of concept that such an effect is EV dependent and high methylated miRNA mediated has been gathered by evaluation of the luciferase activity of five episomal reporter vectors as in Figure 3A. Notably, as shown in Figure 6B, the EVs produced by shCTR and shMETTL3 cells have different effects, and, specifically, only shCTR EVs downregulate luciferase activity in recipient cells.

To gather direct insight into how EV-delivered miRNA function changes in relation with the methylation status, EVs from shCTR HepG2 cells were tested in recipient murine hepatocytes where the demethylase FTO (both nuclear and cytoplasmic in this cell line; Figure S6A) was pharmacologically inhibited (Figures 6C and S6B). Notably, FTO inhibition impacts the EV-mediated downregulation of the same mRNAs, as demonstrated by messenger RNA sequencing (Figure 6D and File S3). Furthermore, the effect of FTO impairment was tested through a luciferase assay; as shown in Figure 6E, FTO inhibition counteracts EV-delivered miRNA function in recipient mouse hepatocytes. This evidence was formally proven by an equivalent analysis performed in commercial primary bronchial epithelial (HBEpC) recipient cells chosen for not expressing miRNA 122-5p. Here EV-delivered 122-5p function requires endogenous FTO activity, since its inhibition impairs both miRNA/AGO2 interaction and target downregulation. This is shown in Figures 6F and 6G, where AGO2 binding is assessed by CLIP assay and miRNA function by luciferase assay.

These analyses formally demonstrated that EV-delivered miRNA function reacquisition in recipient cells requires endogenous FTO activity.

DISCUSSION

This evidence highlights that epitranscriptomic miRNA modification impacts both cell-autonomous gene expression regulation and cell-to-cell communication.

Data provide evidence that (1) mature miRNAs are modified in a cell-specific manner; (2) m6A modification impairs the interaction between the methylated miRNA fraction and AGO2 and, in turn, their function; (3) mature miRNA m6A modification enhances their extracellular delivery through the EV loader A2B1; and (4) recipient cells utilize EV-miRNA informational content in dependence on the FTO demethylation activity.

m6A modification inhibits intermolecular dsRNA formation[31,32]; this is sufficient to make the RNA accessible to single strand-binding partners,[33] thus impacting RNA function. With respect to miRNA m6A modification, previous data have highlighted that it impacts their biogenesis; indeed, Alarcon et al. have reported that METTL3 depletion results in an upregulation of several primary microRNAs, being detrimental for their processing.[5] Moreover, m6A has been characterized to play a role in mRNA translation impairment,[2,5] and it has been proposed that m6A-mediated structural changes may impact the stability of the RISC complex.[2]

Here, microRNA sequencing analyses allowed us to describe, in HepG2 cells, several highly, lowly, and non-methylated miRNAs that are modified in a distinct manner in a second hepatoma cell line, Hep3B. Similar observations suggesting a cell-specific regulation of the miRNA methylation profile have been made in mouse liver and hepatoma cells. The miRNAs analyzed here share two previously defined consensus sequences (RACH and METTL3) that are also found significantly in human (32% and 21%, respectively) and murine (32% and 18%, respectively) miRNome fractions.

These observations (1) extend the occurrence of the methylation to a broad repertoire of miRNAs and (2) suggest that many miRNAs have the potential to be methylated in a dynamic manner in different cell types.

The impact of methylation on AGO2-miRNA association has not been previously characterized in depth. A structural analysis[34,35] has indicated that the miRNA/AGO2 interaction is a dynamic multi-step process, and, in this frame, it appears conceivable that m6A could influence miRNA conformation and, in turn, AGO2 binding. Moreover, Konno et al. predicted, by a molecular mechanics approach, that, for miRNA 17-5p and let-7a-5p, m6A causes a structural change of the RISC complex due to variation in the binding interaction between AGO2 and these miRNAs.[2] Here, data show that the m6A-dependent functional dampening of miRNA regulation is mediated by an impairment of its association with the key adaptor protein of the silencing complex.

Indeed, a CLIP analysis demonstrated that the interaction between six miRNAs (high methylated in this cellular model) and AGO2 occurs only in response to METTL3 silencing. Moreover, *in vitro* RNA pull-down with fully methylated and non-methylated

Figure 4. m6A-modification mediates miRNA loading in the EV compartment

(A) Comparison between methylation status of the indicated mature miRNAs in the intracellular (cell) and EV compartment (EVs) by MeRIP qPCR analysis on HepG2 cells.

(B) EV miRNA levels in shCTR and shMETTL3 HepG2 cells analyzed by RT-qPCR. Data are expressed as ratio of miRNA expression in EVs with respect to the intracellular compartment (shCTR arbitrary value 1). Results are shown as the mean ± SEM of six independent experiments.

(C) EV miRNA levels upon METTL3 inhibitor (STM2457) treatment, analyzed by RT-qPCR. Data are expressed as ratio of miRNA expression in EVs with respect to the intracellular compartment. Results are shown as the mean ± SEM of six independent experiments. Data are considered statistically significant with $p < 0.05$ (two-tailed Mann-Whitney paired test). p value: * < 0.05; ** < 0.01; *** < 0.001.

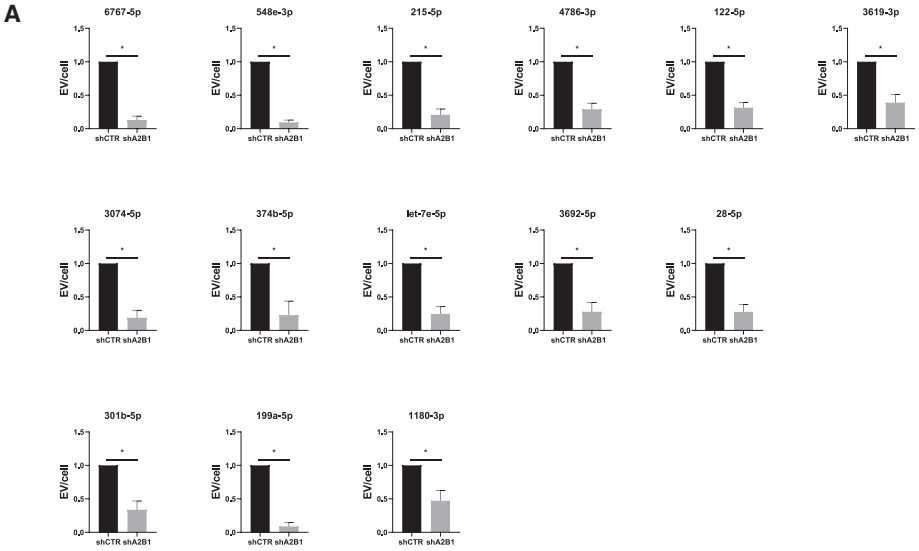

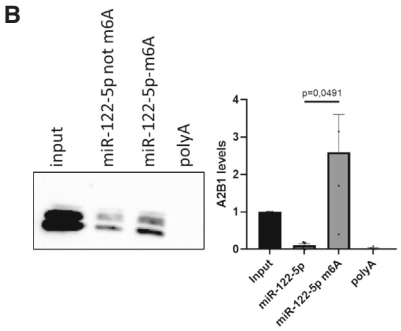

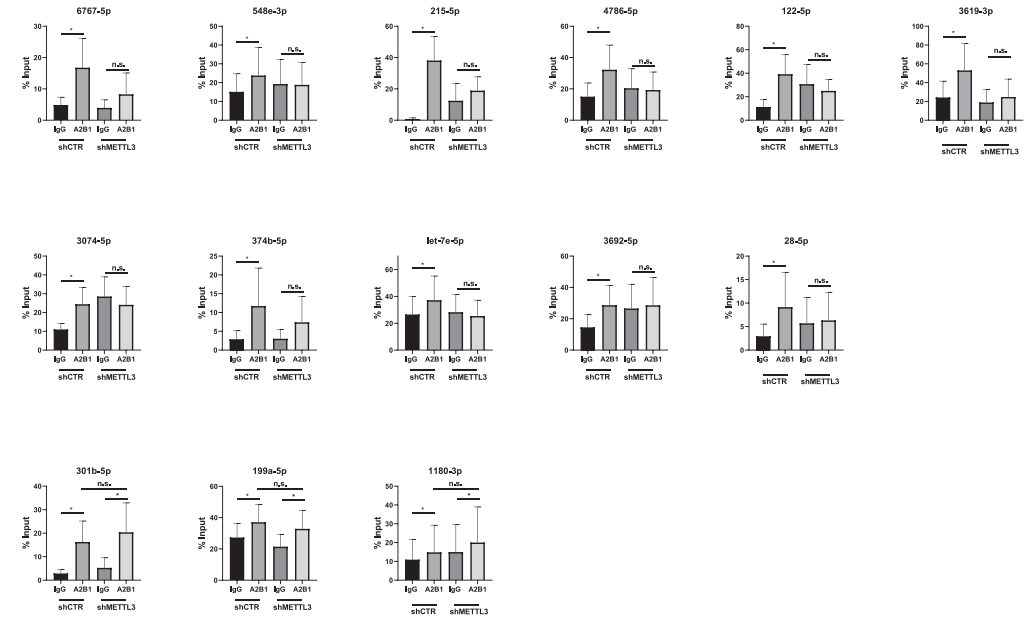

(legend on next page)

miR122-5p and miR6767-5p clearly shows that the methylation interferes with AGO2/miRNA interaction.

Notably, while miRNAs' expression is nowadays considered a diagnostic functional biomarker,[36] these findings highlight the need of an in-depth analysis of the miRNAs' cell-specific epitranscriptomic modifications. To address the paradox of miRNA expression related to their functional inhibition, we investigated the hypothesis that m6A modification influenced miRNA loading in EVs.

The evaluation of miRNA methylation level in cells vs. EVs obtained by MeRIP and native mass spectrometry highlighted an enrichment of the methylated miRNA fraction in EVs. Furthermore, a direct correlation between miRNA methylation and EV loading has been explored by a genetic (METTL3 silencing) and pharmacologic (STM2457 METTL3 inhibitor) approach. miRNA EV loading is known to take advantage of multiple pathways; to shed light on the m6A-dependent mechanism of miRNA EV loading, we focused on the regulatory role mediated by the RBP A2B1. We analyzed the effect of A2B1 silencing in our cellular model, confirming its loading role. More interesting is that we found that METTL3 silencing influenced A2B1/miRNAs interaction; specifically, while for some miRNAs, this binding appears to be independent from methylation (conceivably being only sequence dependent), for others, demethylation reduces A2B1 recruitment.

Together, these data indicate that m6A impairs AGO2/miRNA interaction and, therefore, intracellular gene regulation and influences A2B1-mediated miRNA EV compartmentalization. This additional mechanism does not rule out that A2B1 loading may be also m6A independent and that m6A-dependent loading may be paralleled by an effect of m6A methylation on other RBP-dependent mechanisms of miRNA retention/export. Therefore, m6A should also be taken into account when considering the relation between the miRNA levels and their intracellular gene regulation potential and/or their export to target cells.

Finally, the gene expression and luciferase analysis demonstrated that EV-delivered methylated miRNAs are functional in recipient cells and that they require endogenous FTO-mediated demethylation for both AGO2 recruitment and function on their targets. This extends the previously described role of erasers (e.g., FTO) to one of mediators of cell-to-cell communication, conceivably implying a demethylation step within the EV internalization route. Of note, despite tumultuous literature reporting EV miRNA-mediated impact on physiological and pathological processes, several crucial aspects of the molecular mechanisms allowing miRNAs to exert their function in receiving cells (e.g., how much miRNA is delivered and how miRNAs reassociate with Argonaute protein) remain not fully understood; their comprehension will enhance the EV translational potential.

Overall, these data provide evidence of an epitranscriptomic regulatory mechanism that distributes the miRNA function between intracellular and cell-to-cell communication, allowing producing cells to restrict functional effects to target cells.

These observations, made in specific experimental systems, shall conceivably be important for the RNA biology community as well as for medical researchers currently investigating the informational role of EVs in cell-to-cell communication and considering them as a promising tool for RNA therapy.

This thought is supported by a motif search analysis on mature miRNAs that indicated that a share of them bear methylation motifs; this ensemble could, in principle, be methylated in different cell types and under pathophysiological conditions, thus dynamically impacting cell-autonomous vs. multicellular regulatory pathways.

Limitations of the study

The observation that m6A modification is cell specific and is not dependent on the relative expression levels of each miRNA suggests regulatory pathways as yet unaddressed. Moreover, in this study, as for the multitude of reports on EV-mediated miRNA function in recipient cells, no evidence of the molecular machinery promoting miRNA/RISC reassociation in receiving cells is provided. Similarly, the FTO activity on methylated miRNAs is only deduced from the use of inhibitors, and no evidence of its cellular localization is provided.

STAR★METHODS

Detailed methods are provided in the online version of this paper and include the following:

- KEY RESOURCES TABLE
- RESOURCE AVAILABILITY
  - Lead contact
  - Materials availability
  - Data and code availability
- EXPERIMENTAL MODEL AND STUDY PARTICIPANT DETAILS
  - Cell culture conditions
- METHOD DETAILS
  - Lentiviral and retroviral packaging and infections
  - MeRIP (methylated RNA immunoprecipitation)
  - Sequencing
  - Small RNA-Sequencing data analysis
  - Motifs search and enrichment analyses
  - RNA-sequencing data analysis
  - MazF assay
  - Cell transfection
  - Luciferase assay
  - miRNA pull-down
  - Protein extraction and western-blot analysis
  - MTS assay
  - CLIP (crosslinking RNA immunoprecipitation)
  - RNA dot blot analysis
  - Native mass spectrometry
  - Extracellular vesicles purification and recipient cell treatment

Figure 5. m6A-modification mediates A2B1-dependent miRNA loading in the EV compartment

(A) EV miRNA levels in shCTR and shA2B1 HepG2 cells, analyzed by RT-qPCR. Results are shown as the mean ± SEM of six independent experiments.

(B) RNA pull-down with the unmethylated and methylated miR122-5p (miR122-5p and miR122-5p-m6A, respectively), followed by western blot (left) and densitometric analysis (right) for A2B1 signals. Data are representative of four independent experiments.

(C) CLIP of A2B1 protein in shCTR and shMETTL3 HepG2 cells. Data are shown as the mean ± SEM of six independent experiments and are represented as % input.

(A and C) Data are considered statistically significant with $p < 0.05$ (two-tailed Mann-Whitney paired test). p value: * < 0.05; ** < 0.01; *** < 0.001.

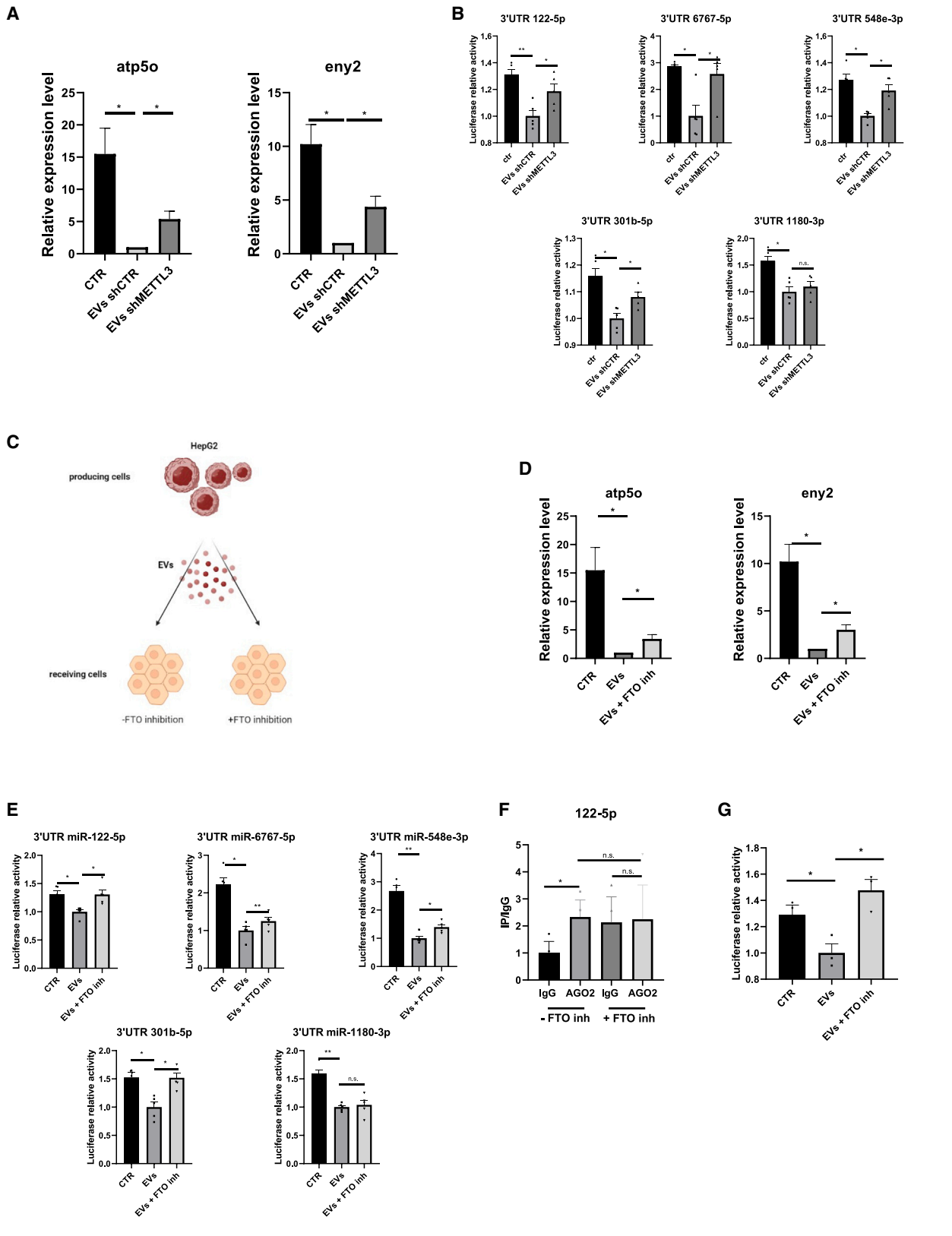

(legend on next page)

- RNA extraction, reverse transcription, quantitative polymerase chain reaction
- Immunofluorescence

- QUANTIFICATION AND STATISTICAL ANALYSIS

SUPPLEMENTAL INFORMATION

Supplemental information can be found online at https://doi.org/10.1016/j.celrep.2024.114369.

ACKNOWLEDGMENTS

We thank Prof. Alessandro Fatica and Dr. Zaira Ianniello for providing the lentiviral vector for METTL3 silencing and for comments and suggestions, Dr. Laura Santangelo for preparing retroviral particles for A2B1 silencing, Prof. Rossella Maione for critical discussions, Dr. Francesco Marocco, Dr. Sara Minotti, and Dr. Clemens Zwergel for editing assistance, Dr. Chiara Agrati and Dr. Veronica Bordoni for providing HBEpC cells, and Dr. Ana Boskovic and Dr. Cornelius Gross (EMBL Monterotondo, Italy) for advice on wide-range analyses. The research leading to these results has been supported by Associazione Italiana per la Ricerca sul Cancro (AIRC) IG 26290 to M.T.; by Sapienza University of Rome (RG11916B6A9C42C7) (to M.T.); Seed Pnr 2021, Sapienza University of Rome (RG120172B73EDDC5 and RM12218166AEFC72) (to C.B.), Grandi Attrezzature Scientifiche 2021 n. GA12117A8711CC9F (INCENTIVE MS) to A.M., and NativePolyPharma to F.F. S.G. is supported by the AIRC Post-Doctoral Fellowship.

AUTHOR CONTRIBUTIONS

Conceptualization, S.G., M.T., and C.B.; methodology, S.G., D.D., A.C., and F.F.; investigation, S.G., D.D., A.C., F.F., A.R., G.G.T., M.T., and C.B.; visualization, S.G., D.D., A.C., F.F., and C.B.; data analysis, S.G., D.D., A.C., and A.T.; funding acquisition, M.T. and C.B.; supervision, D.D., A.M., M.T., and C.B.; writing – original draft, S.G., M.T., and C.B.; editing, D.D., A.C., A.R., F.F., A.T., M.T., and C.B.

DECLARATION OF INTERESTS

The authors declare no competing interests.

Received: October 13, 2023
Revised: April 19, 2024
Accepted: May 31, 2024

REFERENCES

1. Esteller, M., and Pandolfi, P.P. (2017). The Epitranscriptome of Noncoding RNAs in Cancer. Cancer Discov. *7*, 359–368. https://doi.org/10.1158/2159-8290.CD-16-1292.
2. Konno, M., Koseki, J., Asai, A., Yamagata, A., Shimamura, T., Motooka, D., Okuzaki, D., Kawamoto, K., Mizushima, T., Eguchi, H., et al. (2019). Distinct methylation levels of mature microRNAs in gastrointestinal cancers. Nat. Commun. *10*, 3888. https://doi.org/10.1038/s41467-019-11826-1.
3. Liang, Y., Ding, S., Wang, X., Hu, C., Zhang, Y., Hu, Y., Zhang, Y., Kong, H., Xia, W., Jing, Q., et al. (2021). Adipose/Connective Tissue From Thyroid-Associated Ophthalmopathy Uncovers Interdependence Between Methylation and Disease Pathogenesis: A Genome-Wide Methylation Analysis. Front. Cell Dev. Biol. *9*, 716871. https://doi.org/10.3389/fcell.2021.716871.
4. Alarcon, C.R., Goodarzi, H., Lee, H., Liu, X., Tavazoie, S., and Tavazoie, S.F. (2015). HNRNPA2B1 Is a Mediator of m(6)A-Dependent Nuclear RNA Processing Events. Cell *162*, 1299–1308. https://doi.org/10.1016/j.cell.2015.08.011.
5. Alarcon, C.R., Lee, H., Goodarzi, H., Halberg, N., and Tavazoie, S.F. (2015). N6-methyladenosine marks primary microRNAs for processing. Nature *519*, 482–485. https://doi.org/10.1038/nature14281.
6. Berulava, T., Rahmann, S., Rademacher, K., Klein-Hitpass, L., and Horsthemke, B. (2015). N6-adenosine methylation in MiRNAs. PLoS One *10*, e0118438. https://doi.org/10.1371/journal.pone.0118438.
7. Barbieri, I., and Kouzarides, T. (2020). Role of RNA modifications in cancer. Nat. Rev. Cancer *20*, 303–322. https://doi.org/10.1038/s41568-020-0253-2.
8. Lan, Y., Liu, B., and Guo, H. (2021). The role of M(6)A modification in the regulation of tumor-related lncRNAs. Mol. Ther. Nucleic Acids *24*, 768–779. https://doi.org/10.1016/j.omtn.2021.04.002.
9. Liu, J., Dou, X., Chen, C., Chen, C., Liu, C., Xu, M.M., Zhao, S., Shen, B., Gao, Y., Han, D., et al. (2020). N (6)-methyladenosine of chromosome-associated regulatory RNA regulates chromatin state and transcription. Science *367*, 580–586. https://doi.org/10.1126/science.aay6018.
10. Desrosiers, R., Friderici, K., and Rottman, F. (1974). Identification of methylated nucleosides in messenger RNA from Novikoff hepatoma cells. Proc. Natl. Acad. Sci. USA *71*, 3971–3975. https://doi.org/10.1073/pnas.71.10.3971.
11. Dominissini, D., Moshitch-Moshkovitz, S., Schwartz, S., Salmon-Divon, M., Ungar, L., Osenberg, S., Cesarkas, K., Jacob-Hirsch, J., Amariglio, N., Kupiec, M., et al. (2012). Topology of the human and mouse m6A RNA methylomes revealed by m6A-seq. Nature *485*, 201–206. https://doi.org/10.1038/nature11112.

Figure 6. EV-miRNA function on recipient cells requires demethylation

(A) Relative expression level of the indicated mRNAs in D3 hepatocytes treated with HepG2-derived EVs (shCTR or shMETTL3), analyzed by RT-qPCR. Data are shown as the mean ± SEM of five independent experiments. EV shCTR arbitrary value 1.

(B) Luciferase relative activity on D3 hepatocytes transfected with luciferase vectors containing the 3′ UTR of miR-122-5p, miR-6767-5p, miR-548e-3p, miR301b-5p, and miR-1180-3p and treated with HepG2-derived EVs (shCTR or shMETTL3). Data are shown as the mean ± SEM of five independent experiments. EV shCTR arbitrary value 1.

(C) Schematic of the experiment setting relative to (D)–(G). (EVs, cells treated with shCTR EVs; −FTO inh, cells treated with DMSO; +FTO inh, cells treated with FB23-2, an FTO inhibitor).

(D) Relative expression level of the indicated mRNAs, analyzed by RT-qPCR in D3 hepatocytes treated as illustrated in (C). CTR, cells not treated with EVs. Data are shown as the mean ± SEM of five independent experiments. EVs arbitrary value 1.

(E) Luciferase relative activity on D3 hepatocytes transfected with luciferase vectors as in (B) and treated with HepG2-derived EVs and FTO inhibitor as in (C). Data are shown as the mean ± SEM of five independent experiments. EVs arbitrary value 1.

(F) CLIP of AGO2 protein in HBEpC cells treated with HepG2-derived EVs in the presence or absence of FTO inhibitor (FTO inh). Data are shown as the mean ± SEM of three independent experiments and are represented as (IP/IgG). −FTO IgG arbitrary value 1.

(G) Luciferase relative activity on HBEpC cells transfected with the luciferase vector containing the 3′ UTR targeted by miR-122-5p and treated as in (C). Data are shown as the mean ± SEM of three independent experiments. EVs arbitrary value 1.

(A–E) Data are considered statistically significant with $p < 0.05$ (ANOVA followed by a post hoc test). p value: * < 0.05; ** < 0.01; *** < 0.001.

12. Perry, R.P., and Kelley, D.E. (1973). Messenger RNA turnover in mouse L cells. J. Mol. Biol. *79*, 681–696. https://doi.org/10.1016/0022-2836(73)90071-5.

13. Liu, J., Yue, Y., Han, D., Wang, X., Fu, Y., Zhang, L., Jia, G., Yu, M., Lu, Z., Deng, X., et al. (2014). A METTL3-METTL14 complex mediates mammalian nuclear RNA N6-adenosine methylation. Nat. Chem. Biol. *10*, 93–95. https://doi.org/10.1038/nchembio.1432.

14. Dominissini, D., Moshitch-Moshkovitz, S., Salmon-Divon, M., Amariglio, N., and Rechavi, G. (2013). Transcriptome-wide mapping of N(6)-methyladenosine by m(6)A-seq based on immunocapturing and massively parallel sequencing. Nat. Protoc. *8*, 176–189. https://doi.org/10.1038/nprot.2012.148.

15. Linder, B., Grozhik, A.V., Olarerin-George, A.O., Meydan, C., Mason, C.E., and Jaffrey, S.R. (2015). Single-nucleotide-resolution mapping of m6A and m6Am throughout the transcriptome. Nat. Methods *12*, 767–772. https://doi.org/10.1038/nmeth.3453.

16. Meyer, K.D., Saletore, Y., Zumbo, P., Elemento, O., Mason, C.E., and Jaffrey, S.R. (2012). Comprehensive analysis of mRNA methylation reveals enrichment in 3' UTRs and near stop codons. Cell *149*, 1635–1646. https://doi.org/10.1016/j.cell.2012.05.003.

17. Moshitch-Moshkovitz, S., Dominissini, D., and Rechavi, G. (2022). The epitranscriptome toolbox. Cell *185*, 764–776. https://doi.org/10.1016/j.cell.2022.02.007.

18. Xu, C., Liu, K., Ahmed, H., Loppnau, P., Schapira, M., and Min, J. (2015). Structural Basis for the Discriminative Recognition of N6-Methyladenosine RNA by the Human YT521-B Homology Domain Family of Proteins. J. Biol. Chem. *290*, 24902–24913. https://doi.org/10.1074/jbc.M115.680389.

19. Zheng, G., Dahl, J.A., Niu, Y., Fedorcsak, P., Huang, C.M., Li, C.J., Vågbø, C.B., Shi, Y., Wang, W.L., Song, S.H., et al. (2013). ALKBH5 is a mammalian RNA demethylase that impacts RNA metabolism and mouse fertility. Mol. Cell *49*, 18–29. https://doi.org/10.1016/j.molcel.2012.10.015.

20. Fu, Y., Jia, G., Pang, X., Wang, R.N., Wang, X., Li, C.J., Smemo, S., Dai, Q., Bailey, K.A., Nobrega, M.A., et al. (2013). FTO-mediated formation of N6-hydroxymethyladenosine and N6-formyladenosine in mammalian RNA. Nat. Commun. *4*, 1798. https://doi.org/10.1038/ncomms2822.

21. Li, Y., Cheng, X., Chen, Y., Zhou, T., Li, D., and Zheng, W.V. (2021). METTL3 facilitates the progression of hepatocellular carcinoma by modulating the m6A level of USP7. Am. J. Transl. Res. *13*, 13423–13437.

22. Barbieri, I., Tzelepis, K., Pandolfini, L., Shi, J., Millán-Zambrano, G., Robson, S.C., Aspris, D., Migliori, V., Bannister, A.J., Han, N., et al. (2017). Promoter-bound METTL3 maintains myeloid leukaemia by m(6)A-dependent translation control. Nature *552*, 126–131. https://doi.org/10.1038/nature24678.

23. Yankova, E., Blackaby, W., Albertella, M., Rak, J., De Braekeleer, E., Tsagkogeorga, G., Pilka, E.S., Aspris, D., Leggate, D., Hendrick, A.G., et al. (2021). Small-molecule inhibition of METTL3 as a strategy against myeloid leukaemia. Nature *593*, 597–601. https://doi.org/10.1038/s41586-021-03536-w.

24. Kozomara, A., and Griffiths-Jones, S. (2011). miRBase: integrating microRNA annotation and deep-sequencing data. Nucleic Acids Res. *39*, D152–D157. https://doi.org/10.1093/nar/gkq1027.

25. Fromm, B., Høye, E., Domanska, D., Zhong, X., Aparicio-Puerta, E., Ovchinnikov, V., Umu, S.U., Chabot, P.J., Kang, W., Aslanzadeh, M., et al. (2022). MirGeneDB 2.1: toward a complete sampling of all major animal phyla. Nucleic Acids Res. *50*, D204–D210. https://doi.org/10.1093/nar/gkab1101.

26. Santangelo, L., Giurato, G., Cicchini, C., Montaldo, C., Mancone, C., Tarallo, R., Battistelli, C., Alonzi, T., Weisz, A., and Tripodi, M. (2016). The RNA-Binding Protein SYNCRIP Is a Component of the Hepatocyte Exosomal Machinery Controlling MicroRNA Sorting. Cell Rep. *17*, 799–808. https://doi.org/10.1016/j.celrep.2016.09.031.

27. Villarroya-Beltri, C., Gutiérrez-Vázquez, C., Sánchez-Cabo, F., Pérez-Hernández, D., Vázquez, J., Martin-Cofreces, N., Martinez-Herrera, D.J., Pascual-Montano, A., Mittelbrunn, M., and Sánchez-Madrid, F. (2013). Sumoylated hnRNPA2B1 controls the sorting of miRNAs into exosomes through binding to specific motifs. Nat. Commun. *4*, 2980. https://doi.org/10.1038/ncomms3980.

28. Garcia-Martin, R., Wang, G., Brandão, B.B., Zanotto, T.M., Shah, S., Kumar Patel, S., Schilling, B., and Kahn, C.R. (2022). MicroRNA sequence codes for small extracellular vesicle release and cellular retention. Nature *601*, 446–451. https://doi.org/10.1038/s41586-021-04234-3.

29. Wu, B., Su, S., Patil, D.P., Liu, H., Gan, J., Jaffrey, S.R., and Ma, J. (2018). Molecular basis for the specific and multivariant recognitions of RNA substrates by human hnRNP A2/B1. Nat. Commun. *9*, 420. https://doi.org/10.1038/s41467-017-02770-z.

30. Amicone, L., Spagnoli, F.M., Späth, G., Giordano, S., Tommasini, C., Bernardini, S., De Luca, V., Della Rocca, C., Weiss, M.C., Comoglio, P.M., et al. (1997). Transgenic expression in the liver of truncated Met blocks apoptosis and permits immortalization of hepatocytes. EMBO J. *16*, 495–503. https://doi.org/10.1093/emboj/16.3.495.

31. Gao, Y., Vasic, R., Song, Y., Teng, R., Liu, C., Gbyli, R., Biancon, G., Nelakanti, R., Lobben, K., Kudo, E., et al. (2020). m(6)A Modification Prevents Formation of Endogenous Double-Stranded RNAs and Deleterious Innate Immune Responses during Hematopoietic Development. Immunity *52*, 1007–1021.e8. https://doi.org/10.1016/j.immuni.2020.05.003.

32. Xiao, Z., Wang, S., Tian, Y., Lv, W., Sheng, H., Zhan, M., Huang, Q., Zhang, Z., Zhu, L., Zhu, C., et al. (2023). METTL3-mediated m6A methylation orchestrates mRNA stability and dsRNA contents to equilibrate γδ T1 and γδ T17 cells. Cell Rep. *42*, 112684. https://doi.org/10.1016/j.celrep.2023.112684.

33. Liu, N., Dai, Q., Zheng, G., He, C., Parisien, M., and Pan, T. (2015). N(6)-methyladenosine-dependent RNA structural switches regulate RNA-protein interactions. Nature *518*, 560–564. https://doi.org/10.1038/nature14234.

34. Schirle, N.T., and MacRae, I.J. (2012). The crystal structure of human Argonaute2. Science *336*, 1037–1040. https://doi.org/10.1126/science.1221551.

35. Schirle, N.T., Sheu-Gruttadauria, J., and MacRae, I.J. (2014). Structural basis for microRNA targeting. Science *346*, 608–613. https://doi.org/10.1126/science.1258040.

36. Condrat, C.E., Thompson, D.C., Barbu, M.G., Bugnar, O.L., Boboc, A., Cretoiu, D., Suciu, N., Cretoiu, S.M., and Voinea, S.C. (2020). miRNAs as Biomarkers in Disease: Latest Findings Regarding Their Role in Diagnosis and Prognosis. Cells *9*, 276. https://doi.org/10.3390/cells9020276.

37. Schindelin, J., Arganda-Carreras, I., Frise, E., Kaynig, V., Longair, M., Pietzsch, T., Preibisch, S., Rueden, C., Saalfeld, S., Schmid, B., et al. (2012). Fiji: an open-source platform for biological-image analysis. Nat. Meth. *9* (*7*), 676–682. https://doi.org/10.1038/nmeth.2019.

38. Atwood, A., DeConde, R., Wang, S.S., Mockler, T.C., Sabir, J.S.M., Ideker, T., and Kay, S.A. (2011). Cell-autonomous circadian clock of hepatocytes drives rhythms in transcription and polyamine synthesis. Proc. Natl. Acad. Sci. USA *108*, 18560–18565. https://doi.org/10.1073/pnas.1115753108.

39. Battistelli, C., Garbo, S., Riccioni, V., Montaldo, C., Santangelo, L., Vandelli, A., Strippoli, R., Tartaglia, G.G., Tripodi, M., and Cicchini, C. (2021). Design and Functional Validation of a Mutant Variant of the LncRNA HOTAIR to Counteract Snail Function in Epithelial-to-Mesenchymal Transition. Cancer Res. *81*, 103–113. https://doi.org/10.1158/0008-5472.CAN-20-1764.

40. Rodriguez-Hernandez, M.A., Chapresto-Garzón, R., Cadenas, M., Navarro-Villarán, E., Negrete, M., Gómez-Bravo, M.A., Victor, V.M., Padillo, F.J., Muntané, J., et al. (2020). Differential effectiveness of tyrosine kinase inhibitors in 2D/3D culture according to cell differentiation, p53 status and mitochondrial respiration in liver cancer cells. Cell Death Dis. *11*, 339. https://doi.org/10.1038/s41419-020-2558-1.

41. Sorci, M., Ianniello, Z., Cruciani, S., Larivera, S., Ginistrelli, L.C., Capuano, E., Marchioni, M., Fazi, F., and Fatica, A. (2018). METTL3 regulates WTAP

protein homeostasis. Cell Death Dis. *9*, 796. https://doi.org/10.1038/s41419-018-0843-z.

42. Martin, M. (2011). Cutadapt removes adapter sequences from high-throughput sequencing reads. EMBnet. j. *17*, 10. https://doi.org/10.14806/ej.17.1.200.
43. Langmead, B., Trapnell, C., Pop, M., and Salzberg, S.L. (2009). Ultrafast and memory-efficient alignment of short DNA sequences to the human genome. Genome Biol. *10*, R25. https://doi.org/10.1186/gb-2009-10-3-r25.
44. Danecek, P., Bonfield, J.K., Liddle, J., Marshall, J., Ohan, V., Pollard, M.O., Whitwham, A., Keane, T., McCarthy, S.A., Davies, R.M., et al. (2021). Twelve years of SAMtools and BCFtools. GigaScience *10*, giab008. https://doi.org/10.1093/gigascience/giab008.
45. Ritchie, M.E., Phipson, B., Wu, D., Hu, Y., Law, C.W., Shi, W., and Smyth, G.K. (2015). limma powers differential expression analyses for RNA-sequencing and microarray studies. Nucleic Acids Res. *43*, e47. https://doi.org/10.1093/nar/gkv007.
46. Law, C.W., Chen, Y., Shi, W., and Smyth, G.K. (2014). voom: Precision weights unlock linear model analysis tools for RNA-seq read counts. Genome Biol. *15*, R29. https://doi.org/10.1186/gb-2014-15-2-r29.
47. Tremblay, B. (2023). universalmotif: Import, Modify, and Export Motifs with R. package version 1.20.0. https://doi.org/10.18129/B9.bioc.universalmotif.
48. Dobin, A., Davis, C.A., Schlesinger, F., Drenkow, J., Zaleski, C., Jha, S., Batut, P., Chaisson, M., and Gingeras, T.R. (2013). STAR: ultrafast universal RNA-seq aligner. Bioinformatics *29*, 15–21. https://doi.org/10.1093/bioinformatics/bts635.
49. Li, B., and Dewey, C.N. (2011). RSEM: accurate transcript quantification from RNA-Seq data with or without a reference genome. BMC Bioinf. *12*, 323. https://doi.org/10.1186/1471-2105-12-323.
50. Love, M.I., Huber, W., and Anders, S. (2014). Moderated estimation of fold change and dispersion for RNA-seq data with DESeq2. Genome Biol. *15*, 550. https://doi.org/10.1186/s13059-014-0550-8.
51. Dahm, G.M., Gubin, M.M., Magee, J.D., Techasintana, P., Calaluce, R., and Atasoy, U. (2012). Method for the isolation and identification of mRNAs, microRNAs and protein components of ribonucleoprotein complexes from cell extracts using RIP-Chip. J. Vis. Exp., 3851. https://doi.org/10.3791/3851.
52. Quetschlich, D., Esser, T.K., Newport, T.D., Fiorentino, F., Shutin, D., Chen, S., Davis, R., Lovera, S., Liko, I., Stansfeld, P.J., et al. (2021). NaViA: a program for the visual analysis of complex mass spectra. Bioinformatics *37*, 4876–4878. https://doi.org/10.1093/bioinformatics/btab436.
53. Witwer, K.W., Goberdhan, D.C., O'Driscoll, L., Théry, C., Welsh, J.A., Blenkiron, C., Buzás, E.I., Di Vizio, D., Erdbrügger, U., Falcón-Pérez, J.M., et al. (2021). Updating MISEV: Evolving the minimal requirements for studies of extracellular vesicles. J. Extracell. Vesicles *10*, e12182. https://doi.org/10.1002/jev2.12182.
54. Mathieu, M., Névo, N., Jouve, M., Valenzuela, J.I., Maurin, M., Verweij, F.J., Palmulli, R., Lankar, D., Dingli, F., Loew, D., et al. (2021). Specificities of exosome versus small ectosome secretion revealed by live intracellular tracking of CD63 and CD9. Nat. Commun. *12*, 4389. https://doi.org/10.1038/s41467-021-24384-2.

STAR★METHODS

KEY RESOURCES TABLE

REAGENT or RESOURCE	SOURCE	IDENTIFIER
Antibodies		
m6A antibody	Synaptic System	Cat # 202 003; RRID:AB_2279214
Normal Rabbit IgG	Millipore	Cat # 12-370; RRID:AB_145841
Anti-METTL3 antibody	Abcam	Cat # 195352; RRID:AB_2721254
Anti-hnRNP A2B1 antibody	Abcam	Cat # Ab31645; RRID:AB_732978
Anti-Glyceraldehyde-3-Phosphate Dehydrogenase	Millipore	Cat # MAB-374; RRID:AB_2107445
Anti Mouse Ago2	Wako	Cat # 018-22021; RRID:AB_2096310
Goat Anti-Rabbit IgG (H + L)-HRP Conjugate	Bio-Rad Laboratories	Cat # 172-1019; RRID:AB_11125143
Goat Anti-Mouse IgG (H + L)-HRP Conjugate	Bio-Rad Laboratories	Cat # 170-6516; RRID:AB_11125547
Normal Mouse IgG	Millipore	Cat # 12-371; RRID:AB_145840
Anti-CD9 Antibody	Millipore	Cat # CBL 162; RRID:AB_2075914
CD81 Antibody	Santa-Cruz Biotechnology	Cat # sc-166029; RRID:AB_2275892
Anti-LAMP1 antibody	Abcam	Cat # Ab25630; RRID:AB_470708
Calnexin Antibody	Novus Biologicals	Cat # NB100-1965; RRID:AB_10002123
Fatso (C-3)	Santa Cruz Biotechnology	Cat # sc-271713; RRID:AB_10707817
Chemicals, peptides, and recombinant proteins		
Dimethyl sulfoxide	Sigma	Cat #D2650-5X10MG
Fetal Bovine Serum	Gibco	Cat # 10270
DMEM	Gibco	Cat # 21969-035
RPMI-1640	Gibco	Cat # 31870-025
EGF	Peprotech	Cat # AF-100-15-1MG
IGFII	Peprotech	Cat # 100-12-100UG
Insulin	Merck	Cat #M376497001
Penicillin/Streptomycin	Euroclone	Cat # ECB3001D
L-Glutamine	Euroclone	Cat # ECB3000D
Collagen from rat tail	Life Technologies	Cat # A1048301
Bronchial tracheal epithelial growth medium	Sigma-Aldrich	Cat # 511/500
FB23-2	MedChemExpress	Cat # HY-127103
STM2457	MedChemExpress	Cat # HY-134836
Doxyciclin	Sigma-Aldrich	Cat #D9891
Tris	Sigma	Cat #T1503-5KG
NaCl	Carlo Erba	Cat # 479687
NP-40	Fluka	Cat # 74385
EDTA	Carlo Erba	Cat # 405463
SDS	Fisher Bioreagents	Cat # BP166-500
Dynabeads™ Protein G	Invitrogen	Cat # 100040
Dynabeads™ Protein A	Invitrogen	Cat # 100020
Bovine Serum Albumin	Promega	Cat #R396E
Chloroform	Carlo erba	Cat # 438601
Qiazol	Qiagen	Cat # 79306
Glycogen	Sigma-Aldrich	Cat #G8751
Sodium Acetate	Invitrogen	Cat # AM9740
Ethanol	Carlo Erba	Cat # 414605
Interferase™ -MazF enzyme	Takara	Cat # 2415A

(*Continued on next page*)

Continued

REAGENT or RESOURCE	SOURCE	IDENTIFIER
Lipofectamine LTX Reagent	Thermo Fisher Scientific	Cat # 15338100
FuGENE® HD Transfection Reagent	Promega	Cat #E2311
Dynabeads™ M-280 Streptavidin	Thermo Fisher	Cat # 11205D
KCl	Carlo Erba	Cat # 471177
$MgCl_2$	Carlo Erba	Cat # 459337
DTT	Thermo Fisher Scientific	Cat #R0861
EGTA	Fluka	Cat # 03778
Glycerol	Carlo Erba	Cat # 453752
RNAse inhibitor	Promega	Cat #N261B
Leupeptin	ThermoFisher	Cat # 78435
Aprotinin	Sigma	Cat # A4529
PMSF	Sigma	Cat #P76-26
Sodium Orthovanadate	Sigma	Cat #S6508
Yeast tRNA	Life Technologies	Cat # 15401011
Laemli	Alfa Aesar	Cat #J61337
Triton X-100	Auros Organics	Cat # 327372500
Acrylamide	Bio-Rad Laboratories	Cat # 1610148
APS	Sigma	Cat # A-7460
Temed	Sigma	Cat # 203-744-6
Nitrocellulose membrane	Bio-Rad Laboratories	Cat # 1620115
Nylon Membrane	Amersham	Cat # RPN.203N
Glycine	Fisher Bioreagents	Cat # BP381-5
Methanol	Merck	Cat # 32213-2,5L-M
Tween 20	Merck	Cat # 8.22184.0500
Ponceau	Sigma	Cat #P7170
Nonfat-dried milk	PanReac AppliChem	Cat # A0830,0500
PageRuler™ Plus Prestained Protein Ladder	Thermo Scientific	Cat # 26619
ECL	Bio-Rad Laboratories	Cat # 1705062
Spike-In	NORGEN	Cat # 59000
GoTaq qPCR MasterMix	Promega	Cat # A600A
Formamide	Sigma	Cat # F-9037
Formaldehyde	AppliChem	Cat # A0877,0250
Methylene blue	Sigma	Cat #M9140-25G
PBS	Euroclone	Cat # ECB4004L
DAPI	ThermoFisher Scientific	Cat # 62248
Critical commercial assays		
Look-out Mycoplasma PCR Detection Kit	Merck	Cat # MP0035
NEBNext Ultra II Directional RNA Library Prep kit	New England Biolabs	Cat #E7760L
NEXTFLEX Small RNA Seq Kit v3	Bioo Scientific	Cat # 5132-05
Dual-Luciferase® Reporter Assay System	Promega	Cat #E1910
CellTiter 96® AQueous One Solution Cell Proliferation Assay	Promega	Cat #G3580
ReliaPrep™ RNA Miniprep Systems	Promega	Cat #Z6112
iScript™ cDNA Synthesis Kit	Bio-Rad Laboratories	Cat # 1708891
miRNeasy Mini Kit	Qiagen	Cat # 1038703
RNeasy MinElute Cleanup Kit	Qiagen	Cat # 74204
mistiCq	Sigma-Aldrich	Cat # MIRRT-100RXN

(*Continued on next page*)

Continued

REAGENT or RESOURCE	SOURCE	IDENTIFIER
Deposited data		
RNA and small RNA-sequencing	This paper	Zenodo (https://zenodo.org/deposit/7594655)
Experimental models: Cell lines		
HepG2	ATCC	N/A
HepG2 shCTR	this paper	N/A
HepG2 shMETTL3	this paper	N/A
Hep3B	ATCC	N/A
Bw1J	ATCC	N/A
D3	https://doi.org/10.1093/emboj/16.3.495	N/A
HBEpC	ATCC	N/A
Oligonucleotides		
Primers for miRNA expression are listed in Table S1	This paper	N/A
Primers for gene expression analyses are listed in Table S2	This paper	N/A
Recombinant DNA		
pLKOTet-On Lentiviral shRNA clones (shMETTL3)	Dharmacon	Cat # TRCN0000289812
pLKOTet-On Lentiviral shRNA clones (Non-Target shRNA Control)	Dharmacon	Cat # SHC202 TRC2
pmirGLO Dual-Luciferase miRNA Target Expression Vector	Promega	Cat #E1330
Software and algorithms		
ImageJ/FiJI	NIH Schindelin et al.[37]	https://imagej.net/software/fiji/
Prism 9 GraphPad	https://www.graphpad.com/	N/A
ChemiDoc Imaging System	Bio-Rad	Cat# 12003153
Image Lab Software	Bio-Rad	Cat# 12012931
FastQC tool	N/A	v0.11.8
miRBase	https://doi.org/10.1093/nar/gkq1027	Release 22.
cutadapt	https://doi.org/10.14806/ej.17.1.200	v4.1
Bowtie	https://doi.org/10.1186/gb-2009-10-3-r25	v1.3.1
Samtools	https://doi.org/10.1093/gigascience/giab008	v1.3.1
limma R package	https://doi.org/10.1093/nar/gkv007	v3.54.0
miRGeneDB	https://doi.org/10.1093/nar/gkab1101	2.1
UniversalMotif R package	https://doi.org/10.18129/B9.bioc.universalmotif	1.20.0.
Python	N/A	v3.8.5
FastQC tool	N/A	v0.11.8
STAR	https://doi.org/10.1093/bioinformatics/bts635	v2.7.0e
Gencode	N/A	release M30
RSEM	https://doi.org/10.1186/1471-2105-12-323	v1.3.
tximport package	N/A	v1.12.3
DESeq2 package	https://doi.org/10.1186/s13059-014-0550-8	v1.24.0
R	https://doi.org/10.1093/nar/gkv007	v3.54.0
Xcalibur	Thermo Scientific	3.0
NaViA	https://doi.org/10.1093/bioinformatics/btab436	N/A
Nikon NIS-elements software	Nikon Corporation	N/A

RESOURCE AVAILABILITY

Lead contact

Further information and requests for resources and reagents should be directed to and will be fulfilled by the lead contact, Cecilia Battistelli (cecilia.battistelli@uniroma1.it).

Materials availability

This study generated new cell lines (HepG2 shCTR and HepG2 shMETTL3) and we are available to share under request without restrictions.

Data and code availability

- RNA-sequencing data has been deposited to Zenodo (https://zenodo.org/deposit/7594655). The deposited data will be made publicly accessible by the paper's publication date.
- This paper does not report original code.
- Any additional information required to reanalyze the data reported in this paper is available from the lead contact upon request.

EXPERIMENTAL MODEL AND STUDY PARTICIPANT DETAILS

Cell culture conditions

Human HepG2 and Hep3B, murine BW1J hepatoma cells and Non-tumorigenic D3[30] hepatocytes were grown as previously described.[38–40] In detail, HepG2, Hep3B and BW1J were grown in DMEM supplemented by 10% FBS, L-Glutamine (2mM) and Penicillin (100u/ml)/Streptomycin (100μg/ml). D3 cells were grown on collagen I coated plates in RPMI supplemented by 10% FBS, L-Glutamine (2mM), Penicillin (100u/ml)/Streptomycin (100μg/ml) and Insulin (10μg/ml), IGFII (30 ng/ml) and EGF (50 ng/ml). HBEpC cells were grown in Bronchial/Tracheal Epithelial Growth Medium (511-500, Sigma-Aldrich) supplemented with 10% FBS and 10% DMSO. All cell lines were tested for mycoplasma using the DAPI staining and the LookOut Mycoplasma PCR Detection Kit (MP0035, Merck). All cell lines were authenticated after thawing by morphology check, cell proliferation rate evaluation and species verification by PCR. Bacteria contamination was excluded. FTO inhibitor FB23-2 (resuspended in DMSO) treatment was performed at a concentration of 20 μM for 48h on D3 and HBEpC cells. METTL3 inhibitor STM2457 (resuspended in DMSO) treatment was performed at a concentration of 5 μM for 72h on HepG2 cells.

METHOD DETAILS

Lentiviral and retroviral packaging and infections

Lentiviral particles were prepared from mission pLKOTet-On Lentiviral shRNA clones (Merck KGaA, Darmstadt, Germany) TRCN0000289812 (shMETTL3), and SHC202 TRC2 (Non-Target shRNA Control) as in.[41] The induction of shRNA was obtained by doxycycline treatment (2 μg/mL) for 72h. Retroviral particles were prepared as in.[26] shA2B1 sequence is: 5′-GAT CCC CCC ATA CCA TCA ATG GTC ATT TCA AGA GAA TGA CCA TTG ATG GTA TGG TTT TTA-3'.

MeRIP (methylated RNA immunoprecipitation)

MeRIP was performed in accordance to,[14] with some modifications of the protocol. Antibody against m6A (202 003; Synaptic System) or Normal Rabbit IgG (12–370; Millipore) was added to the IP buffer (10 mM Tris [pH 7.5], 150 mM NaCl, 0.5% Nonidet P-40) and then incubated with protein A magnetic beads. miRNAs were eluted with elution buffer (5 mM Tris-HCl pH 7.5, 1 mM EDTA, 0.05% SDS) extracted using the phenol-chloroform method, purified, and then analyzed with qRT-PCR. For primer details see Table S2. MeRIP on mRNAs was performed in accordance with.[23] Primers details are reported in Table S1.

Sequencing

mRNA samples were prepared using the NEBNext Ultra II Directional RNA Library Prep kit with the NEBNext Poly(A) mRNA Magnetic Isolation Module as per manufacturer instructions. Samples were standardized to 10 ng input material, with a 1:100 adapter dilution, 15 min fragmentation time, and 16 PCR cycles. Samples were pooled and sequenced with the Illumina NextSeq 500 High 75 cycle kit.

Small RNA samples were prepared following the NEXTFLEX Small RNA Seq Kit v3 as per manufacturer instructions. Samples were standardized to 1 ng input material, with a 1:10 adapter dilution and 25 PCR cycles. Samples were pooled and an additional 0.8x SPRI bead cleanup was performed to remove adapter contamination. Two biological replicates per condition were sequenced with the Illumina NextSeq 500 High 75 cycle kit.

Small RNA-Sequencing data analysis

The fastq files from Illumina Platform were assessed for quality by using FastQC tool (v0.11.8) and trimmed for NEXTFLEX adapter sequences with cutadapt (v4.1).[42] Bowtie (v1.3.1)[43] was used to align the trimmed reads on mature microRNAs. Homo Sapiens

mature microRNAs from miRBase (Release 22.1)[24] were used as reference for the MeRIP human shCTR and MeRIP human shMETTL3. The spike-in sequence (cel-miR-39-3p) was included in the Homo Sapiens miRbase reference before Bowtie indexing. The trimmed reads with 1 mismatch in the first 10 bases and reporting less than 5 reportable alignments were considered in the count. Only 1 alignment was reported per read, considering the Bowtie best-to-worst order. Samtools (v1.3.1)[44] was used to create the expression matrix. Differential expression analysis was performed on microRNAs expressed in at least half of the samples and using the linear modeling implemented in limma R package (v3.54.0)[45] with voom normalization,[46] using as library size the normalized counts from spike-in and the total counts from libraries. miRNAs were considered as methylated (IPed) if, in the shCTR samples, the log2 FC and the FDR adjusted *p*-value for the IP/IgG comparison were >0 and <0.05, respectively, and the log2 FC for the IP/Input comparison was >0, and if, in the shMETTL3 samples, the log2 FC for the IP/IgG comparison was <0 and/or the adjusted *p*-value for the same comparison was >0.05.

Motifs search and enrichment analyses

Human and murine mature miRNA sequences were retrieved from miRBase (Release 22.1); miRNAs annotated as high-confidence in miRBase and/or present in miRGeneDB (release 2.1) database 25 were classified as high-confidence (HC).

Motif enrichment analysis for IPed miRNAs was conducted using two distinct control sets. The first set comprised non-IPed miRNAs with expression levels falling within the range of the IPed miRNAs (only HC miRNAs were used as a control for IPed HC miRNAs). The second set was generated by employing the shuffle_sequences function from the UniversalMotif R package[47] twice on the sequences of IPed miRNAs, creating shuffled sequences while maintaining the original dinucleotide composition. This second strategy was also employed to create the control sets used to evaluate motif enrichment for the full human and mouse mature miRNA sets. RACH, RRACH and DRACH motif occurrences[11,15] were searched within miRNA sequences using regular expressions in Python v3.8.5. METTL3 motif instances were searched by providing the probability matrix, as computed based on the logo reported by Liu and colleagues,[13] to the enrich_motifs function from the UniversalMotif R package,[47] setting the pvalue threshold to 0.01 and restricting the search to the forward strand. Motif enrichment with respect to the control sets was evaluated by using the Fisher's exact test.

RNA-sequencing data analysis

All samples were modeled after the long-rna-seq-pipeline used by the PsychENCODE Consortium and available at https://www.synapse.org/#!Synapse:syn12026837. Briefly, the fastq files from Illumina were assessed for quality by using FastQC tool (v0.11.8) and trimmed for NEXTFLEX adapter sequence and low base call quality (Phred score <30 at ends) with cutadapt (v4.1).[42] Only the reads with length more than 10 were retained. STAR (v2.7.0e)[48] was used to map the trimmed reads and to produce the BAM files in both genomic and transcriptomic coordinates, subsequently sorted using Samtools (v1.9).

GRCm39 was used as the reference genome and the comprehensive gene annotations on the primary assembly from Gencode (release M30) used as gene annotation. Gene and transcript-level quantifications were calculated using RSEM (v1.3.1).[49] Both STAR and RSEM executions were performed using the psychENCODE parameters. RSEM gene and isoform level estimated counts were imported using the tximport package (v1.12.3). Differential gene expression analysis was performed using the DESeq2 package (v1.24.0)[50] and differentially expressed protein coding genes were considered significant if their *p* value after Benjamini & Hochberg correction was <0.05. All the differential analyses were performed by using R (v4.2.2).

MazF assay

MazF assay was performed on 500 ng of miRNAs. After a denaturation step of 70°C for 2 min, the miRNA samples were incubated with mRNA Interferase -MazF enzyme (Takara 2415A) at 37°C for 30 min. After inactivation step at 70°C for 4 min, the samples were purified by phenol/chloroform method, retrotranscribed and analyzed by qPCR.

Cell transfection

D3 and HBEpC cells were transfected with Lipofectamine LTX Reagent (15338100, Thermo Fisher Scientific), according to the manufacturer's protocol. Equal amounts of DNA were used. HepG2 cells were transfected with FuGENE HD Transfection Reagent (E2311, Promega), according to the manufacturer's protocol. HepG2, D3 and HBEpC were transfected with pmirGLO Dual-Luciferase miRNA Target Expression Vector (E1330, Promega) expressing 3′UTR targeted by the analyzed miRNAs.

Luciferase assay

Luciferase assay was performed with Dual-Luciferase Reporter Assay System (Promega) according to the manufacturer's protocol. Plasmid sequences are schematically reported in Figure 3A.

miRNA pull-down

Biotin miRNA pull-down experiments were performed on cytoplasmic extracts. Cells were lysed in hypotonic buffer (10 mM Tris-Cl [pH 7.5], 20 mM KCl, 1.5 mM MgCl2, 5 mM DTT, 0.5 mM EGTA, 5% glycerol, 0.5% NP-40, and 40 U/μL Rnasin [Promega]) supplemented with protease inhibitors (Roche Applied Science). Cytoplasmic extracts were incubated for 1 h at 4°C with 10 nmol synthetic miRNA oligonucleotides containing a biotin modification attached to the 5′ end. Streptavidin beads (DYNABEADS M-280

STREPTAVIDIN, Thermo Fisher), previously blocked with 1 μg/μL yeast tRNA (Roche Applied Science), were added to reaction mixture for 90 min at 4°C, and then the beads were washed five times with 1 mL lysis buffer. Elution was performed with Laemmli buffer.

Protein extraction and western-blot analysis

Cells were lysed in Triton 1X Buffer, subsequently the proteins were analyzed as in.[39] The following primary antibodies were used for immunoblotting: α-METTL3 (195352, Abcam), α-A2B1 (Ab31645; Abcam), α-GAPDH (MAB-374, Millipore Corp.), used as a loading control and α-AGO2 (018–22021; Wako). The immune complexes were detected with horseradish peroxidase-conjugated species-specific secondary antiserum: (α-Rabbit 172–1019 and α-Mouse 170–6516 Bio-Rad Laboratories), then by enhanced chemiluminescence reaction (Bio-Rad Laboratories). Densitometric analysis of protein expression was performed by using the Fiji-Image J image processing package.

MTS assay

shCTR and shMETTL3 HepG2 cells were trypsinized, harvested and seeded onto 96-well flat-bottomed plates at a density of 2,000 cells/well, then incubated at 37°C for 72h in DMEM supplemented with 10% FBS and doxycycline (2μg/ml) to induce shRNA expression. Subsequently, cells were subjected to CellTiter 96 AQueous One Solution Cell Proliferation Assay (Promega), according to the manufacturer's protocol. The absorbance at 490 nm was evaluated to estimate cell number.

CLIP (crosslinking RNA immunoprecipitation)

CLIP was performed as reported in.[51] Cells were subjected to UV cross-linking (one pulse irradiation at 800 mJ/cm^2 in 254 nm Stratalinker [Stratagene 2400, Stratagene])and lysed in ice-cold lysis buffer (10 mM HEPES [pH 7.3], 100 mM KCl, 0.5% NP-40, 5 mM $MgCl_2$, and 0.5 mM DTT) supplemented with protease inhibitors (Leupeptin Thermofisher 78435, Aprotinin Sigma A4529, PMSF Sigma P76-26 and Sodium Orthovanadate Sigma S6508) and RNase inhibitor (Promega N261B). The lysates were centrifuged for 30 min at 13000 RPM and quantified with Bradford assay. 1 mg protein extract was incubated with the specific antibody over-night at 4°C with end-over-end rotation in a final volume of 1.5 mL of NT2 buffer (50 mM Tris-HCl pH 7,4, 150mM NaCl, 1mM $MgCl_2$, 0.05% NP-40). 20 μL protein A/G Dynabeads (Invitrogen) was added for 3 h, followed by three washes with ice-cold LiCl buffer (500 mM LiCl, 0.2% SDS, 0.1% Sodium deoxycholate in PBS 1X). Immunoprecipitated miRNAs were purified using phenol/chloroform extraction and reverse transcribed and analyzed by RT-qPCR amplifications. List of primers is reported in Table S1. Primary antibodies for IP: anti-A2B1 (Ab31645; Abcam), anti-AGO2 (018–22021; Wako) and as negative control Normal Rabbit IgG (12–370; Millipore) or Normal Mouse IgG (12–371; Millipore).

RNA dot blot analysis

miRNA samples were incubated with RNA buffer (formamide, MOPS, and 37% formaldehyde) at 65°C for 5 min and then were added with 20X Saline Sodium Citrate Solution. 100 ng of miRNAs were spotted onto a nylon membrane (Hybond-N, RPN.203N., Amersham) by Bio-dot apparatus (Bio-Rad, USA) and RNA was UV-crosslinked to the membrane. The membrane was incubated with 0.02% Methylene blue and with anti-m6A antibody (202 003, Synaptic System) at 4°C, over-night. The immune complexes were detected as in Western-blot analysis.

Native mass spectrometry

Following extraction, the small RNAs were subjected to dialysis into a solution of 500 mM ammonium acetate pH 7.2 and then analyzed via mass spectrometry under non-denaturing conditions (native MS).

Native MS experiments were performed using a Q Exactive UHMR Hybrid Quadrupole-Orbitrap mass spectrometer (Thermo Fisher) coupled to a nano-electrospray source in negative polarity. The instrument parameters used for MS spectra collection were the following: capillary voltage of 1.2 kV, scan range of 350–5000 m/z, HCD collision voltage of 0 V, source fragmentation of 0 V, and in-source trapping of 0 V. The ion transfer optics were set as follows: injection flatapole of −5 V, inner-flatapole lens of −4 V, bent flatapole of −2 V, and transfer multipole of 0 V. The resolution of the instrument was 200,000 at m/z = 400, the nitrogen pressure in the HCD cell was maintained at approximately 3.0 × 10–10 mbar, and the source temperature was kept at 100°C. Calibration of the instrument was performed using a 2 mg/mL solution of cesium iodide in water. Data were analyzed using the Xcalibur 3.0 (Thermo Scientific) and NaViA[52] software packages.

Extracellular vesicles purification and recipient cell treatment

EVs have been purified according to.[53] In brief, media was collected from donor cells (HepG2) after 48h from seeding. Media was centrifuged at 4°C, 20 min at 2000 rcf, then the supernatant was centrifuged at 4°C, 30 min at 20000 rcf. The media was filtered with 0.2 μm filter and then ultracentrifuged at 4°C, 100000 rcf, 70 min. EVs characterization was performed by western blot for CD9 (CBL 162, Millipore), CD81 (sc-166029, Santa-Cruz), LAMP1 (Ab25630, Abcam) and calnexin (NB100-1965, Novus Biologicals) as in[54] and by EXOID-V1–SC (IZON) analysis. Receiving cells (D3 and HBEpC) were treated with 20 μg/mL (1,67x107 EV/ml) of extracellular vesicles for 24h.

RNA extraction, reverse transcription, quantitative polymerase chain reaction

Total RNA was extracted by ReliaPrep RNA Tissue Miniprep System (Promega, USA) and reverse transcribed with iScriptTM c-DNA Synthesis Kit (Bio-Rad Laboratories Inc., USA). Quantitative polymerase chain reaction (RT-qPCR) analyses were performed according to MIQE guidelines. cDNAs were amplified by qPCR reaction using GoTaq qPCR Master Mix (Promega, Madison, WI, USA). Relative amounts, obtained with 2^(-ΔCt) method, were normalized with respect to the housekeeping gene GAPDH (human) or 18S (murine). For primer details see Table S1 miRNAs were extracted by miRNeasy Mini Kit and RNeasy MinElute Cleanup Kit (QIAGEN) and reverse transcribed with MystiCq microRNA cDNA Synthesis Mix (Sigma-Aldrich). Quantitative polymerase chain reaction (RT-qPCR) analyses were performed according to MIQE guidelines. cDNAs were amplified by qPCR reaction using GoTaq qPCR Master Mix (Promega, Madison, WI, USA). Relative amounts, obtained with 2^(-ΔCt) method, were normalized with respect to the cel-miR-39 Spike-In (59000; NORGEN), previously added into miRNA samples.

Immunofluorescence

Cells were methanol-fixed, permeabilized with 0.1% Triton, incubated with 3% BSA in PBS, treated with mouse α-FTO (Fatso (C-3) sc-271713, Santa Cruz Biotechnology). Alexa CY3-conjugated secondary antibodies (Molecular Probes, Eugene, OR, USA) were used. Nuclei were stained with DAPI (4′,6-diamidino-2-phenylindole; 268298; Calbiochem Merck, Germany). Images were examined with Nikon Microphot-FXA microscope (Nikon Corporation, Japan) equipped with a CCD camera. Digital images were acquired by Nikon NIS-elements software (Nikon Corporation).

QUANTIFICATION AND STATISTICAL ANALYSIS

q-PCR data for the evaluation of miRNA expression and enrichment was performed by two-tailed Mann-Whitney paired test (Wilcoxon test).

ANOVA followed by post-hoc test was used for the experiments in which there is a single control for multiple experimental conditions.

All the statistical details and the number of replicates of each experiment are reported in the figure legends.

Prism 9 GraphPad was used for all the statistical analyses.